iScience

CellPress
OPEN ACCESS

Article

Human fetal dermal fibroblast-myeloid cell diversity is characterized by dominance of pro-healing Annexin1-FPR1 signaling

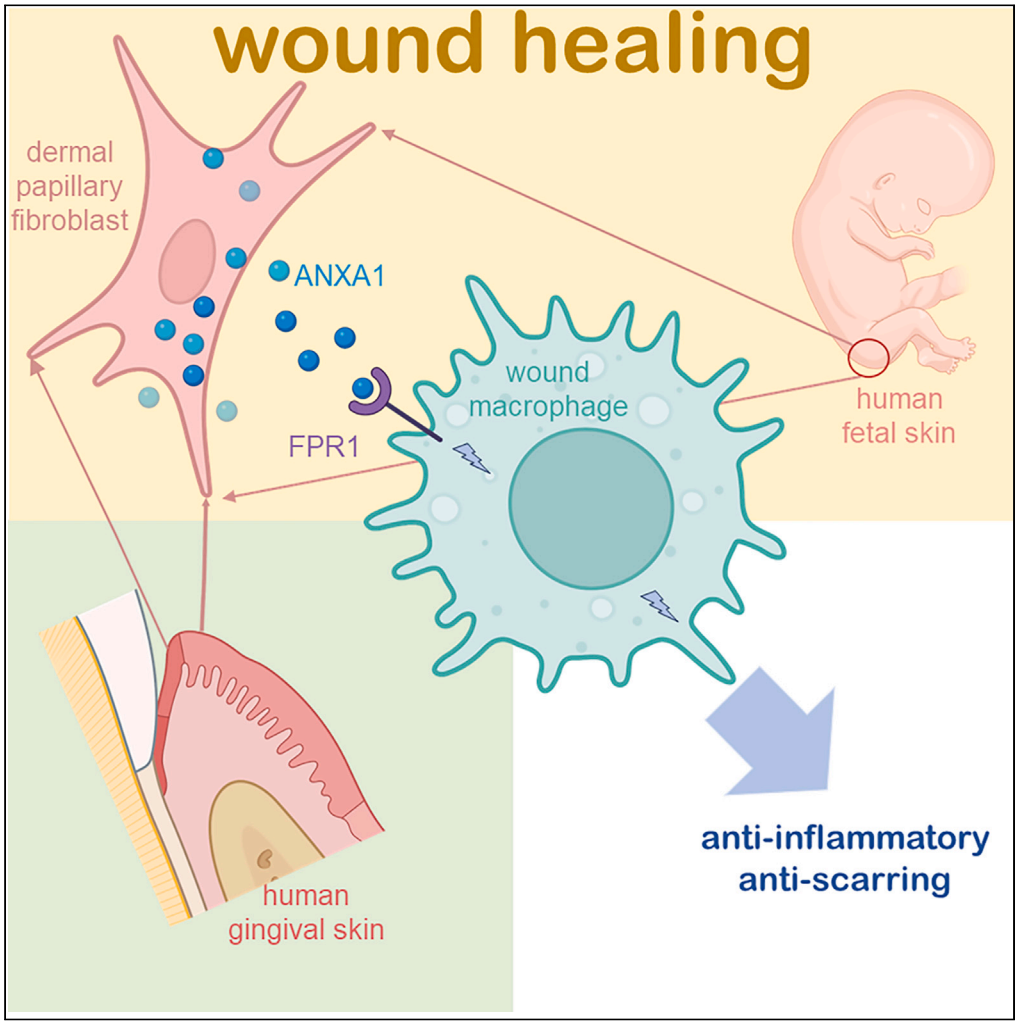

Rajneesh Srivastava, Kanhaiya Singh, Ahmed S. Abouhashem, ..., Subhadip Ghatak, Yi Xuan, Chandan K. Sen

singhk@pitt.edu (K.S.)
c.k.sen@pitt.edu (C.K.S.)

Highlights

Fibroblast subpopulation, unique to human fetal skin, and gingiva minimize scar

Fetal fibroblasts and myeloid cells share energy metabolism gene sets

Annexin1-FPR1 signaling promotes tissue repair and regeneration in fetal skin

Myeloid-specific FPR1 delivery via TNT enhances quality of wound healing

Srivastava et al., iScience *26*, 107533
September 15, 2023
https://doi.org/10.1016/j.isci.2023.107533

iScience

CellPress
OPEN ACCESS

Article

Human fetal dermal fibroblast-myeloid cell diversity is characterized by dominance of pro-healing Annexin1-FPR1 signaling

Rajneesh Srivastava,[1,2] Kanhaiya Singh,[1,2,*] Ahmed S. Abouhashem,[2,3] Manishekhar Kumar,[1,2] Sedat Kacar,[2] Sumit S. Verma,[1,2] Sujit K. Mohanty,[1,2] Mithun Sinha,[2] Subhadip Ghatak,[1,2] Yi Xuan,[1,2] and Chandan K. Sen[1,2,4,*]

SUMMARY

Fetal skin achieves scarless wound repair. Dermal fibroblasts play a central role in extracellular matrix deposition and scarring outcomes. Both fetal and gingival wound repair share minimal scarring outcomes. We tested the hypothesis that compared to adult skin fibroblasts, human fetal skin fibroblast diversity is unique and partly overlaps with gingival skin fibroblasts. Human fetal skin (FS, n = 3), gingiva (HGG, n = 13), and mature skin (MS, n = 13) were compared at single-cell resolution. Dermal fibroblasts, the most abundant cluster, were examined to establish a connectome with other skin cells. Annexin1-FPR1 signaling pathway was dominant in both FS as well as HGG fibroblasts and related myeloid cells while scanty in MS fibroblasts. Myeloid-specific FPR1-ORF delivered in murine wound edge using tissue nanotransfection (TNT) technology significantly enhanced the quality of healing. Pseudotime analyses identified the co-existence of an HGG fibroblast subset with FPR1^{high} myeloid cells of fetal origin indicating common underlying biological processes.

INTRODUCTION

Skin is the largest organ that defends the body against environmental exposure, injury, and infection. Any breach in integrity of the skin triggers a repair process aimed at restoring the barrier function to safeguard life.[1,2] In mature skin (MS) of adults complicated by underlying disease processes, the efficiency of repair is compromised resulting in slow closure and scar outcomes.[3,4] In contrast, the efficiency of fetal skin (FS) repair is high demonstrating blunted inflammatory response[5,6] associated with scar-free regenerative characteristics.[6–9] Interestingly, in adults the gingival tissue repair is such that it shares, albeit to a lesser extent, some of the aforementioned characteristics of fetal repair.[10,11]

Fibroblasts represent one of the most abundant dermal cell types in all three tissues. Recent works have drawn attention to the emergent discipline of dermal fibroblast diversity.[12–16] Novel insight into the lineage,[17] phenotype,[12,18] and plasticity[19,20] of dermal fibroblasts has laid the foundation of a new paradigm addressing the functional significance of fibroblast subtypes in determining wound outcomes.[15,16,21] The physiological wound repair process recruits to the wound-site fibroblasts from distinct micro-environmental niches which include but are not limited to resident skin fibroblasts, bone marrow-derived cells, e.g., fibrocytes, and fibroblast-like cells derived from epithelial, endothelial, perivascular, or adipose tissue.[20,22] Cell transition products such as those of adipocyte-to-mesenchymal and epithelial-to-mesenchymal (EMT) and endothelial-to-mesenchymal (EndMT) are known to exist at the site of injury.[12,23–26] Distinct subpopulations of fibroblast dynamically respond to tissue injury by proliferating, migrating, and adaptively differentiating in response to local cues.[14,27] Wound-responsive fibroblasts include cells rich in Engrailed-1 and Prrx-1. These transcription factors are otherwise known to be markers of developmental lineage.[21,27,28] Our previous work has demonstrated that two-thirds of all granulation tissue fibroblasts, otherwise known to be of mesenchymal origin, are derived from myeloid cells which are likely to be wound macrophages.[20]

The objective of the current work was to study dermal fibroblast diversity in adult/fetal human skin as well as in human gingival tissue. We sought to test the hypothesis that the diversity of human FS fibroblast is unique compared to that of adult skin. FS fibroblast subpopulation that accounts for such uniqueness is

[1]McGowan Institute for Regenerative Medicine, Department of Surgery, University of Pittsburgh School of Medicine, Pittsburgh, PA, USA

[2]Indiana Center for Regenerative Medicine and Engineering, Indiana University Health Comprehensive Wound Center, Indiana University School of Medicine, Indianapolis, IN, USA

[3]Sharkia Clinical Research Department, Ministry of Health, Zagazig, Egypt

[4]Lead contact

*Correspondence: singhk@pitt.edu (K.S.), c.k.sen@pitt.edu (C.K.S.)

https://doi.org/10.1016/j.isci.2023.107533

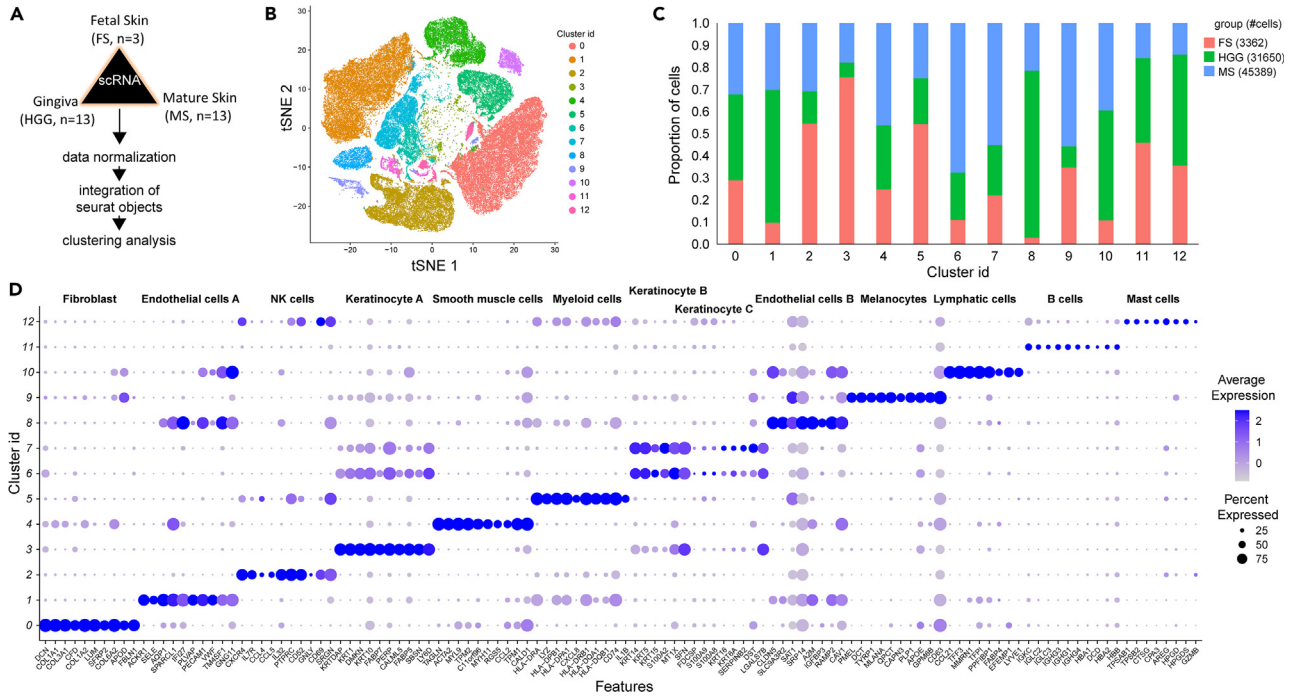

Figure 1. Data mining and clustering analysis identified 13 distinct clusters across studied human tissue types

(A) For this study, scRNA-seq data of human fetal skin (FS, n = 3), gingiva (HGG, n = 13) and mature skin (MS, n = 13) were collected from multiple studies (Table S1). All the processed scRNA-seq samples were quality filtered, normalized using 'SCT-transformation' and stored as Seurat objects in R. Further, these Seurat objects were integrated, and executed for clustering analysis (with resolution 0.25) using Seurat (See STAR Methods).

(B) Resulting cluster of cells were illustrated in tSNE plot, showing the 13 (0–12) clusters with distinct cluster ids.

(C) The proportion of cells per tissue type was illustrated for each cluster as bar graph.

(D) Cluster-specific markers found annotated for each cell type (on top) were shown in dot plot.

shared by the gingiva (HGG), a tissue wherein wound outcomes more closely resemble FS repair as opposed to adult skin repair.

RESULTS

Cellular heterogeneity in FS, HGG, and MS

Single-cell RNA sequencing (scRNA-seq) data analysis of a collection of 80,401 human cells from FS (n = 3), HGG (n = 13), and MS (n = 13) was performed (Table S1; Figure 1A). Integrated analysis using Seurat (version 4.0.2) identified thirteen (0–12) distinct clusters of cells present in FS, HGG, and MS (Figure 1B, see STAR Methods). For each group, the proportion of different cells per cluster was computed and illustrated as stacked proportional plot (Figure 1C; Table S2). These clusters were further characterized based on the average expression of established marker genes (Table S3) and corresponding cell type annotations available in PanglaoDB[29] web server (Figures 1D and S1). Cluster 0, representing 25.4% of all cells, was characterized as fibroblast based on the expression of established marker genes[29–31] (Figure 1D). Cluster 1 was the second most abundant cell type representing 20.3% of all the cells (Figure 1D) for endothelial cells as annotated in PanglaoDB.[29] Cluster 2 was the third most abundant cluster of cells representing 14.9% of all the cells that were characterized as natural killer (NK) cells based on the expression of established marker genes annotated in PanglaoDB[29] (Figure 1D). All other clusters represented less abundant (<8%) cell types including keratinocytes, smooth muscle cells, myeloid cells, melanocytes, lymphatic cells, and other immune cells as depicted in Figures 1C and 1D and Table S2.

Fetal versus mature dermal fibroblast gene expression

Analysis of gene expression profile at single-cell resolution of specific cell types represents a powerful approach to provide insight into their comparative functional characteristics.[32,33] This approach was employed to study cluster 0 (fibroblasts) of fetal compared to MS cells (Figure 2A). This cluster was rich in established markers of fibroblast cells (Figure 2B). Fibroblast for FS and MS groups included 716 (n = 3) and 10,711 (n = 13) cells, respectively (Figure 2C). Differential gene expression analysis comparing fibroblasts of

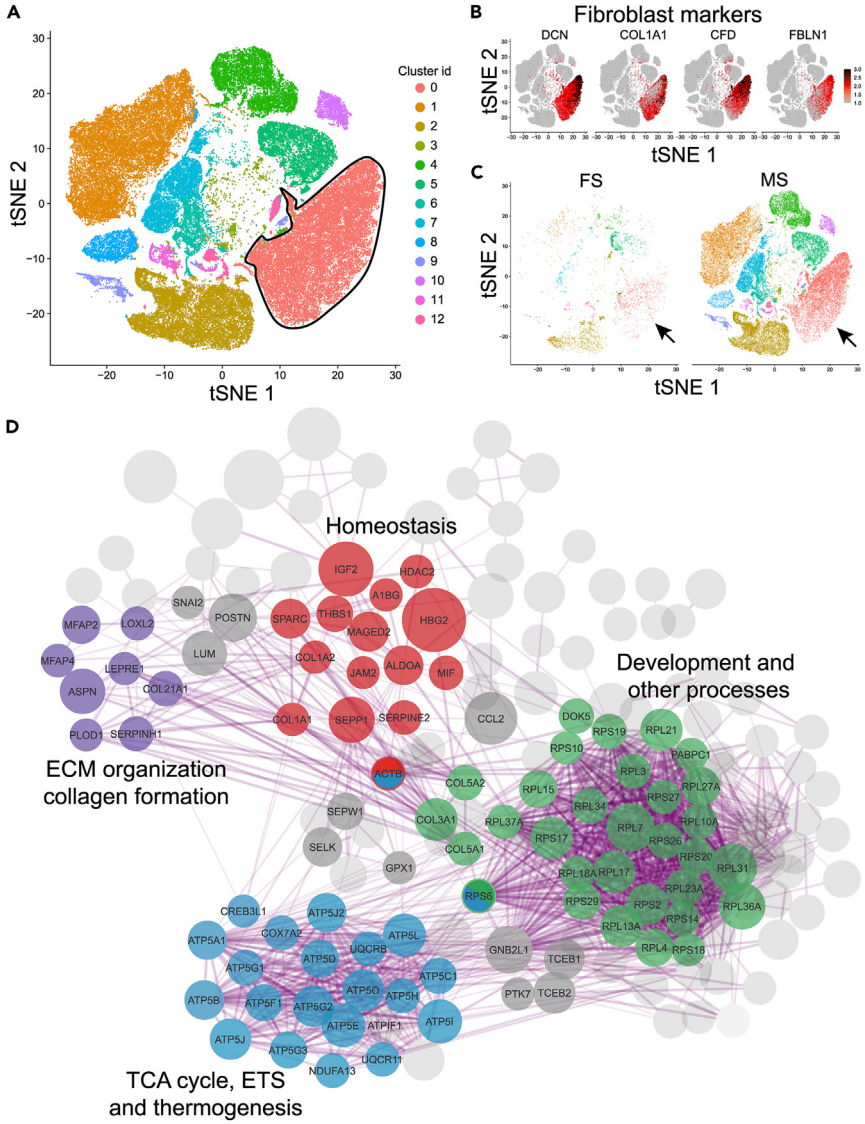

Figure 2. Differential expression analysis of fibroblast cluster

(A) tSNE plot illustrating the distribution of cells for each cluster, with the marked cluster of cells identified as fibroblast cells.

(B) Cells expressing the top 4 signature genes of identified fibroblast cells were shown in tSNE feature plots.

(C) Distribution of fibroblast cells among the original cluster of cells (*panel A*) for FS and MS group were illustrated in tSNE plot. These subclusters were used for differential expression (DE) analysis between FS and MS groups using 'FindMarkers' module (in Seurat package, see STAR Methods).

(D) Functional association analysis of DE genes, high in human fetal skin (FS) fibroblast (log_2 fold change $\geq$0.3 at adjusted p value >0.01,Wilcoxon rank-sum test) was performed using STRING[34] and shown as association network. Highlighted sub-networks were identified as the major subset significantly enriched for mentioned biological processes; i) Extracellular matrix organization, ii) TCA cycle, ETS, thermogenesis iii) Homeostasis and iv) Development and other processes respectively (*please see* Table S5).

these two samples identified 854 differentially expressed genes (DEGs), of which 206 genes were significantly more abundant (log_2 fold change >0.30, adj. p value <0.01) in FS compared to MS (Table S4). These genes were submitted to search tool for recurring instances of neighbouring genes (STRING)[35] database for functional protein association network analysis. The interaction network, thus derived, featured 201 nodes connected by 1,520 edges (Figure 2D). The enriched biological processes associated with these connections are listed (Table S5). Association network analysis revealed four major hubs of network that were

significantly associated with *i)* extracellular matrix organization and collagen organization, *ii)* TCA cycle, ETS, and thermogenesis, *iii)* homeostasis, and *iv)* development processes (Figure 2D).

The dermal cell connectome

Fibroblasts interact with a variety of cells including keratinocytes,[36] endothelial cells,[37] and myeloid cells.[38] We investigated cell-cell communication of all the identified cell clusters in FS, HGG, and MS groups using CellChat.[39] CellChat analysis identified 1,415 (for FS), 1,627 (for HGG), and 2,041 (for MS) cell-cell interactions specifying the respective interaction strengths (Figure S2A). Relative information flow, i.e., cumulative communication probability calculated based on these interactions, was estimated across the groups. Dominant signaling pathways in each group were thus identified (Figure S2B). The relative information flow, estimated as before, was further investigated in the context of incoming and outgoing network across groups (Figure S2C). A strong communication signal pattern for the Annexin signaling pathway was thus identified uniquely for both FS and HGG compared to MS (Figures 3A and S2C). This pathway, enriched in FS and HGG, was primarily annotated with three genes, e.g., *ANXA1* (Annexin A1), *FPR1* (Formyl Peptide Receptor 1), and *FPR2* (Formyl Peptide Receptor 2). *ANXA1* is an important anti-inflammatory signaling ligand.[40–42] *FPR1* is the signaling receptor molecule for ANXA1, characterized for its facilitation of mucosal wound repair via an epithelial FPR1/NADPH oxidase (NOX)1-dependent redox signaling pathway.[43] *FPR*-deficient mice exhibit delayed wound healing[44] underscoring the beneficial role of FPR in tissue repair. In this work, genes associated with the Annexin signaling pathway were investigated for their expression levels across all cell types detected (Figure 3B). The *ANXA1-FPR1* pathway is selectively present in specific cells. While *ANXA1* is ubiquitous, the expression of *FPR1* is limited to myeloid cells of FS and HGG groups. Interestingly, myeloid cells of MS showed sparse expression of *FPR1*. Proximity ligation assay conducted in murine FS, adult skin, and adult HGG directly demonstrated the existence of Annexin1^{+} and FPR1^{+} cells in close proximity with significantly higher abundance in murine FS and gingival tissues compared to adult skin (Figures 3C and 3D). FPR1, which plays a vital role in the function of the innate immune system, also controls several developmental and regenerative processes. Some key examples include promoting migration and differentiation of stem cells,[45] lens development,[46] controlling dynamic plasticity of arteries,[47] and osteogenic induction in hADSCs (human adipose-derived stem cells).[48] In addition, FPR1 activation has been demonstrated to promote wound healing/tissue regeneration, including cell proliferation.[49] Exogenous supplementation of myeloid FPR1 through tissue nanotransfection technology (TNT2.0)[50–53] was able to improve the quality of healing in murine dermal wound model (Figures S3A–S3F). Limited cell-cell communication involving ANXA1-FPR1 in human MS may be viewed as a reflection of restricted regenerative potential of the adult skin compared to FS and gingival tissue.[10,54] In an effort to elucidate the transcriptomic basis of the regenerative properties of FS and HGG, the overall differential interactome was investigated (Figure S2D). The study of differential interaction between fibroblasts and myeloid cells (cluster 0 and 5 respectively, Figure S2E) identified comparable difference in communication of both tissues.

Shared transcriptomic profile of fibroblast and myeloid cells in FS and gingival tissue

CellChat analyses identified Annexin signaling as a major communication pathway between fibroblast and myeloid cellular compartments (Figure 3). Emphasis was therefore placed on analyzing the shared transcriptomic profile of these two cell types with MS as reference tissue (Figure 4A). Seurat-defined subset analyses identified 20,460 fibroblasts and 5,595 myeloid cells across FS, HGG, and MS tissues (Table S2). Differential expression analyses of paired comparisons (FS vs. MS and HGG vs. MS) identified 66 highly abundant DEGs that were shared between fibroblasts of FS and HGG (Figure 4B; Tables S4 and S6). Similar comparative study of the myeloid cell compartment identified 60 elevated DEGs in FS and HGG (Figure 4C; Tables S7 and S8). The intersection analysis of the aforementioned 66 and 60 DEGs identified 35 common genes that were high in both fibroblasts and myeloid cells of FS and HGG (Figures 4D and 4E). Function enrichment analysis of these 35 genes recognized dominance of mitochondrial energy metabolism-related gene ontology (GO) processes (adj. p value = 2.82e-27). Next, we sought to study upregulated DEGs that were unique to each cell compartment. In fibroblasts, 31 such high DEGs were functionally enriched for GO processes such as collagen fibril organization (adj. p value = 1.01e-09, Figure 4F). In myeloid cells 25 such elevated DEGs were functionally enriched for GO processes such as cell chemotaxis (adj. p value = 5.14e-4; Figure 4G).

To test the enrichment of co-expressed modules in FS and HGG groups, the hdWGCNA (high dimensional weighted gene co-expression network analysis)[55,56] tool was employed. This analysis identified 11 co-expression modules for fibroblast and myeloid cells enriched in FS and HGG compared to MS group (Figures S4A–S4C). Each module was compared with previously identified 35 gene set. The pink module contained 91 genes (including 97% genes from Figure 4E) representing co-existence of fibroblast and myeloid cells (Figures S4C

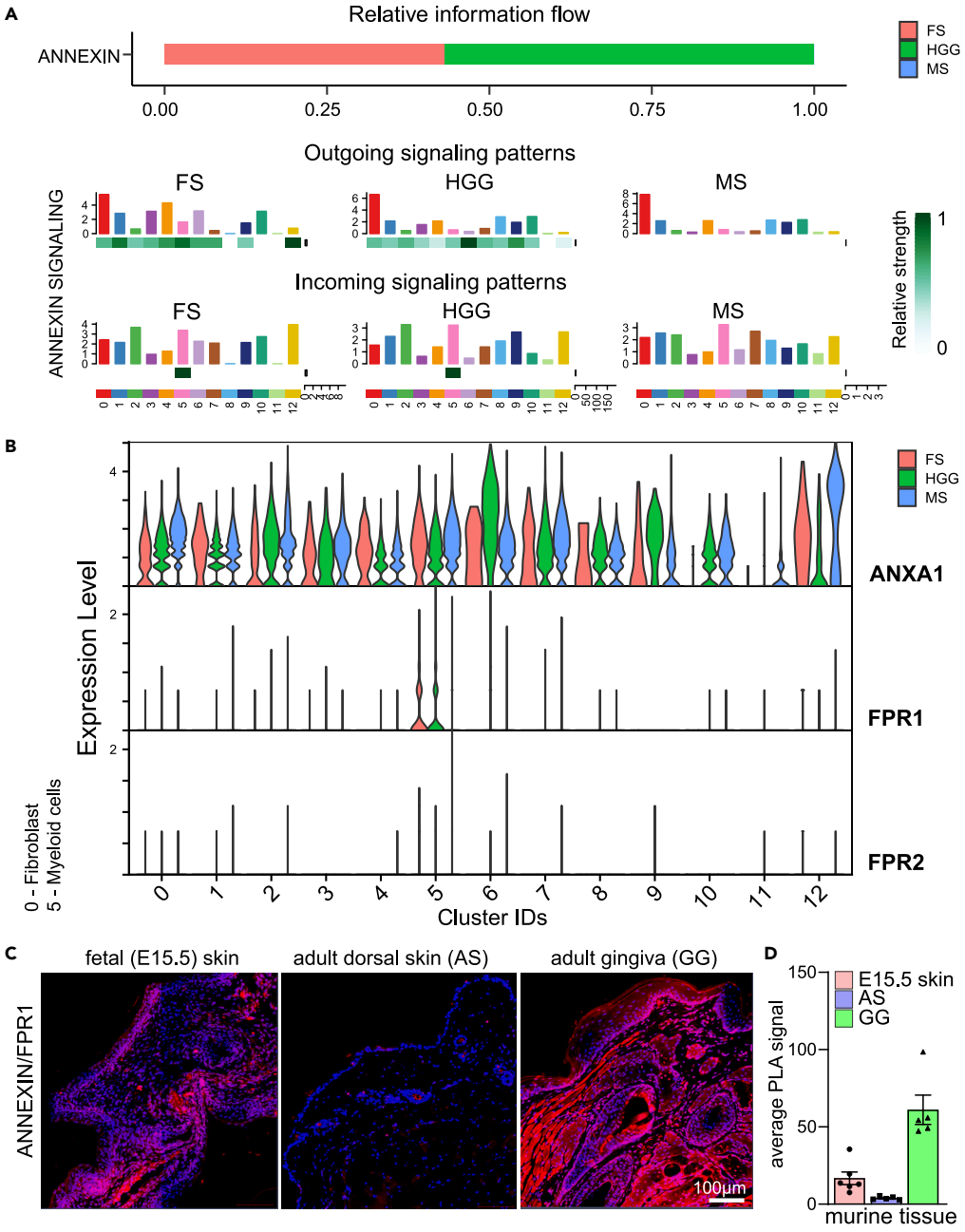

Figure 3. Annexin signaling pathway enriched in FS and HGG groups

(A) Relative information flow of Annexin signaling pathway, ranked based on difference in the cumulative communication probability within the inferred network across FS, HGG and MS groups, were illustrated in proportional stack bar graph. Heatmap showing the comparison of 'outgoing' and 'incoming' signaling patterns associated with each cell population to identify the signaling pathways/ligand-receptors across FS, HGG and MS groups.

(B) Gene expression profile of the signaling molecules, involved in Annexin signaling pathway, were shown as violin plots (split by groups) across all the clusters, where 0 and 5 refers to fibroblast and myeloid cell clusters respectively.

(C) Protein-protein interaction (PPI) between Annexin1 and FPR1 in murine (C57BL/6) skin as indicated by proximity ligation assay. Immunofluorescence (red) is PLA signal that shows protein-protein interactions between Annexin and FPR1 in full thickness skin obtained from fetal (E15.5) skin, adult skin and adult gingiva.

(D) Quantification of Annexin-FPR1 protein-protein interaction by ImageJ. Nuclei are shown stained blue with DAPI. n = 6,5.*p-value <0.05 (one-way ANOVA, followed by Tukey HSD post hoc test). Data represented as mean ± SEM.

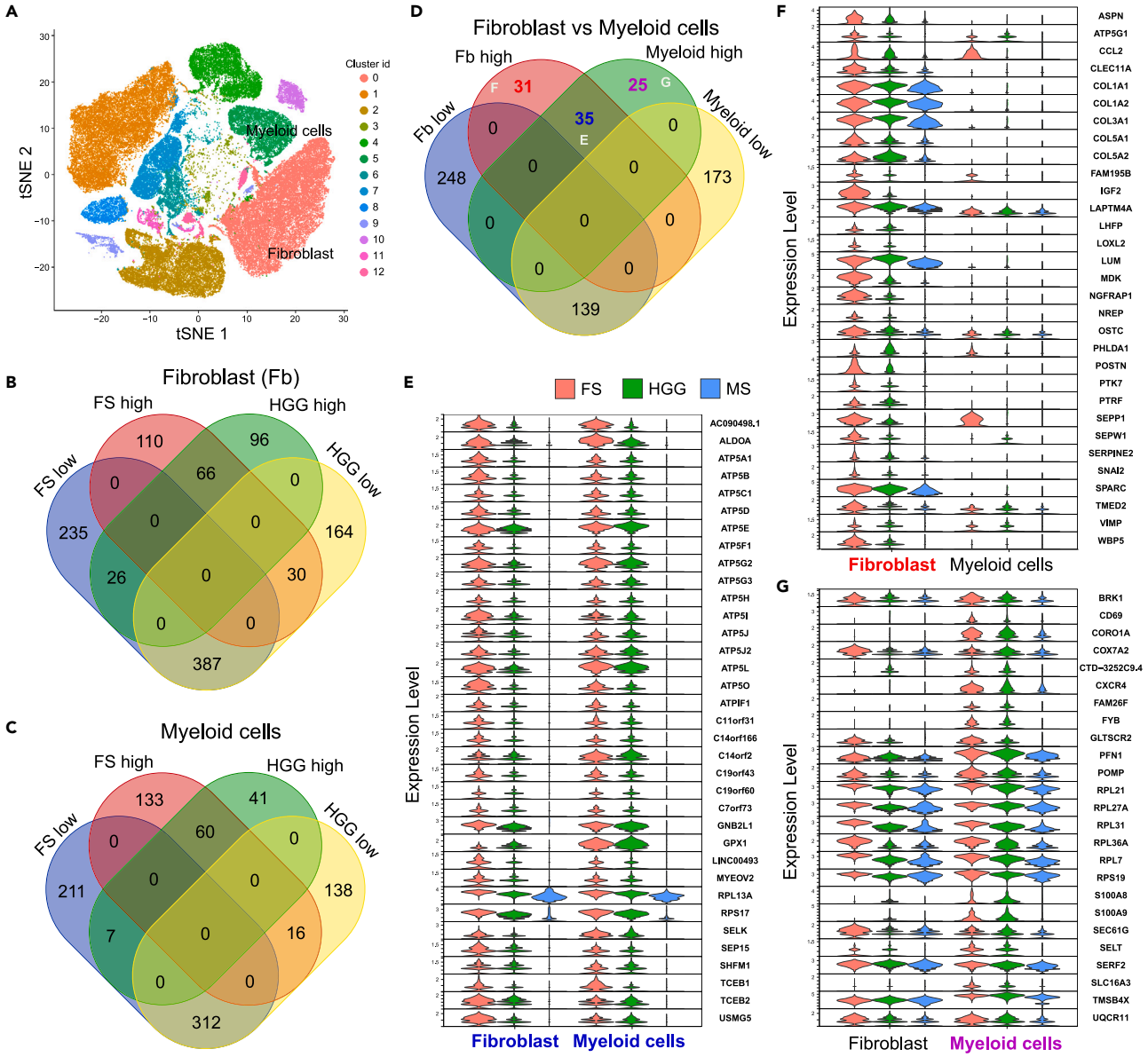

Figure 4. Comparison of differentially expressed gene profiles identified in fibroblast and myeloid cell clusters

(A–C) (A) Distribution of identified clusters of cells with marked fibroblast and myeloid cell clusters were shown as tSNE plot. Venn diagram showing the intersection of differentially expressed (high and low abundant) genes identified in FS and HGG groups compared to MS group (at adj. p value <0.01) for (B) Fibroblast and (C) Myeloid cell clusters.

(D) Venn diagram showing the comparison of differentially expressed 'common' gene pool of the fibroblast (Fb) and myeloid cell clusters identified in both FS and HGG groups.

(E–G) Violin plot showing the expression profile of 'common' gene pool (*as color coded in panel D and labeled in panel E–G*) across groups in fibroblast and myeloid cells.

and S4D). Regulon analysis using pySCENIC (python implementation for Single-Cell rEgulatory Network Inference and Clustering pipeline)[57] identified 23 transcription factors significantly enriched (hypergeometric test, p value <6.55e-02) for targeting the 91 aforementioned genes (Figure S4E).

Relatedness of myeloid cells and fibroblasts of FS and HGG with contrasting MS sub-branch

Analysis of Annexin signaling specifically between fibroblast and myeloid cells of FS and HGG employing the "subset" module followed by re-clustering in Seurat identified (0–5) six subclusters (Figures 5A and

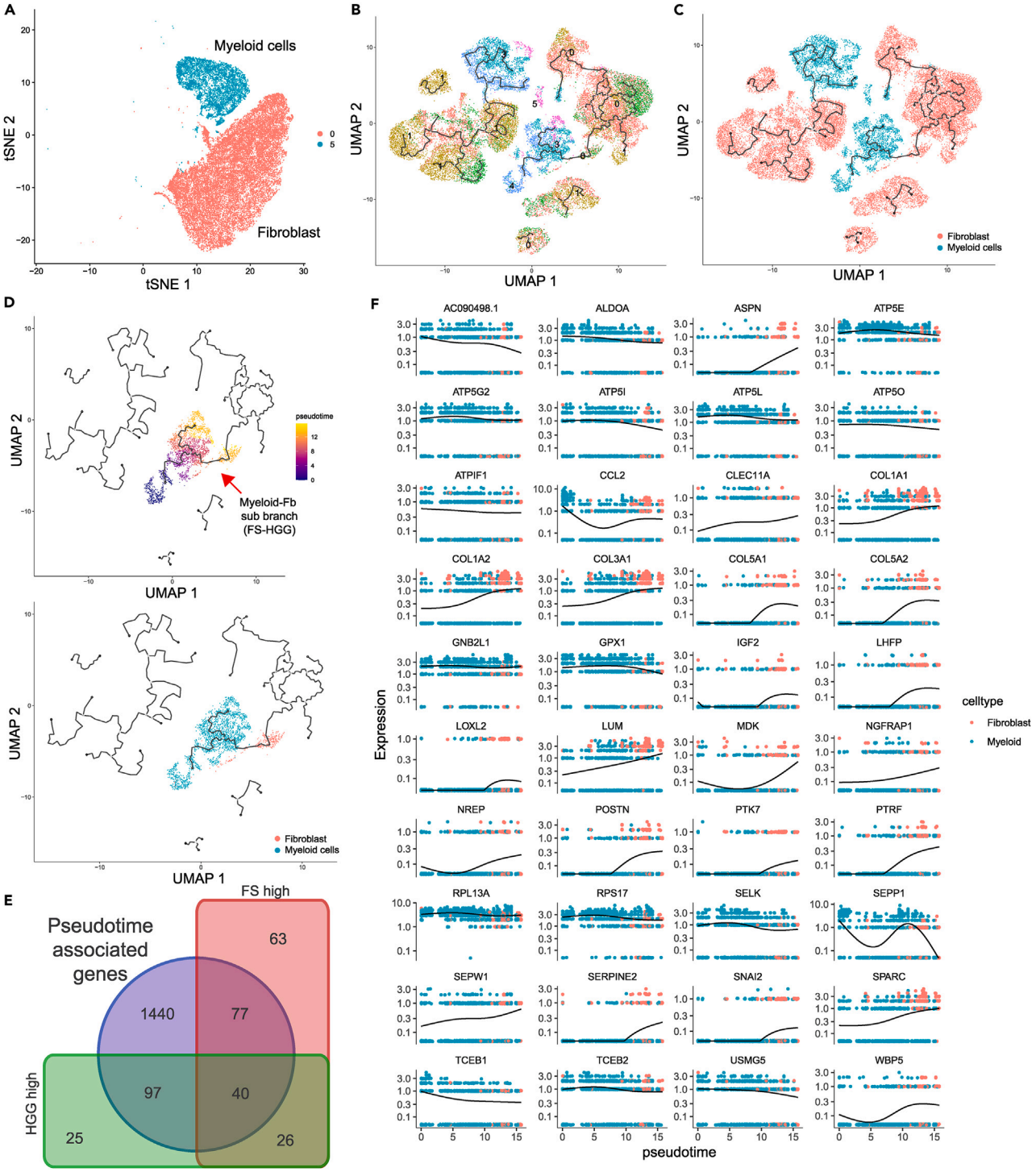

Figure 5. Pseudotime analysis of combined fibroblast and myeloid cell cluster in association with the annexin signaling pathway

(A) Fibroblast and myeloid cell clusters isolated from the original clusters (in Figure 4A) were illustrated as tSNE plot.

(B) UMAP plots showing the distribution of identified sub-clusters in pseudotime space resulting from the trajectory analysis using monocle3.

(C) UMAP plots showing the distribution of fibroblast (red) and myeloid cells (blue) in pseudotime space.

(D) UMAP plots showing the pseudotime trajectory of cells ('Myeloid-Fb sub-branch for FS-HGG groups' (*top)* selected for branchpoint analysis, starting from myeloid cells subcluster 4 (of FS) to fibroblast subcluster 0 of HGG (*bottom*).

Figure 5. *Continued*

(E) Venn diagram showing the comparison of pseudotime associated significant genes (at adj. p value <0.05), identified in the branchpoint analysis, with the significantly upregulated genes of FS and HGG fibroblast clusters (in Figure 4B).

(F) Scatterplot showing the distribution of fibroblast (red) and myeloid cells (blue) along with hybrid expression of the common genes (y axis) with respect to selected pseudotime (x axis) as above (in panel E).

S5A). Based on the expression profile of signature genes,[58–61] the identified subclusters were assigned as three fibroblast and three myeloid cell subsets (Figure S5B). This approach identified subcluster 4, a macrophage subpopulation, as uniquely abundant in FS (Figure S5C). Interestingly, this myeloid subpopulation was *LYZ*^{low} indicating abundance of non-classical myeloid cells in FS (Figures S5B and S5C). In addition, this myeloid subcluster 4 was high on SPP1 (Secreted Phosphoprotein 1, also known as Osteopontin) (Figure S5D). SPP1 is known to be a classical signature gene of fetal macrophages along with the other four markers shown in Figure S5D.[62] Annexin signaling, re-analyzed among these subsets using CellChat, confirmed significant enrichment in FS and HGG groups (Figures S5E and S5F). Connectome, thus derived using CellChat, further identified Fb subcluster 0 to be significantly in communication with myeloid cell subsets 3 and 4 in both FS and HGG groups but not in MS group. Likewise, the expression profile of signaling molecules involved in Annexin signaling showed upregulation in FS and HGG groups across these subsets complementing the previously established connectome (Figure 3). In addition, differential expression analysis identified the annotated fibrotic genes[63–78] to be significantly abundant (adj. p value <0.01) in MS, generally high across all fibroblast subtypes compared to FS (Figure S5G). This analysis leads to the inference that cellular heterogeneity is independent of scarring property in MS.

To understand the dynamics and regulators of cell fate decisions across all six subclusters, pseudo-temporal analysis was conducted using Monocle3.[79] A differentially distributed pattern of these subclusters was thus revealed (Figures 5B, 5C, and S6A). Pseudotime projection identified a dichotomous pattern of cells with distinct sub-branching. Cells expressing SPP1, ANXA1, or FPR1 were projected on pseudotime trajectory (Figure S6B). Based on FPR1 and SPP1 expression profiles (Figure S6B), the trajectory was further partitioned into two distinct myeloid-fibroblast sub-branches, one from FS-HGG (Figure 5D) and the other from MS (Figure S6C). The FS-HGG sub-branch was uniquely distinct from that of MS by the prevalence of SPP1-specific subcluster 4 in pseudotime (Figures 5B, 5D (***bottom***), and S6C).

The aforementioned sub-branches shared a prominent overlapping region of myeloid cells and fibroblasts (Figures 5C and 5D (***top***), Figure S6C). Branchpoint analysis of the overlapped pseudotime trajectory identified 1,654 genes significantly associated with the FS-HGG sub-branch starting from sub-cluster 4 to cluster 0 (Figures 5B–5D; Table S9). These genes demonstrated hybrid expression levels in both fibroblast and myeloid cells of which 40 genes were significantly high in both FS and HGG fibroblast compared to MS (Figure 5E; Table S10). Among these 40 genes, the top three highly expressing genes (log_2 fold change >1.0, adj. p value<0.01) were CCL2 (C-C motif chemokine ligand 2), COL3A1 (collagen 3A1), and LUM (lumican). Each of these three genes was situated in subcluster 0 of both FS and HGG tissues. To decipher the functional significance of these genes in the context of annexing signaling, analysis of interaction network was run using STRING (Figure S6D). To test the significance of the aforementioned 40 genes in MS, the pseudotime trajectory of this sub-branch was analyzed. Only a third of the genes were significantly associated with the marked MS pseudotime space (Figures S6C and S6E; Table S11). Thus, FS and HGG are comparable among themselves and in contrast with MS.

DISCUSSION

Mammalian wound healing shows diverse characteristics depending on the tissue context. The study of such contextual differences in wound healing processes and outcomes can provide critical insight into the conditions necessary to achieve favorable outcomes.[9] Fetal and gingival cutaneous wounds display desirable regenerative healing outcomes.[10,54] In contrast, adult skin wound healing is often complicated and presents undesirable scarring outcomes.[10,54] In fetal healing, the early-gestation repair takes place rapidly with little or no inflammation, faster re-epithelialization, and no scarring.[5,9,80] This phenomenon appears to be intrinsic to FS and independent of the intrauterine environment.[80] Gingival tissue shares the scar-free healing property with fetal tissue, unlikely in MS.[81] Hence, investigation of this contrasting property in tissue context requires a deep understanding of cellular composition in each tissue and the mechanism involved in wound healing.

Fibroblasts, critical drivers of tissue repair, are heterogeneous and a functionally diverse population of cells.[18,36,60,82–85] In the adult skin, a subpopulation of fibroblast contributes to the scarring

phenotype.[18,36,60,86,87] In the FS, fibroblasts play an active role in tissue repair, yet there is no scarring.[88] Gingival tissue repair involves fibroblasts with limited scarring.[89–92] HGG fibroblasts are undifferentiated cells and serve as the main cellular constituent of gingival tissue and are embryo-like cells with the capacity of self-renewal and clonogenicity.[10,93] In this work, fibroblasts are recognized as a prominent cell cluster which is characterized by the expression of fibroblast-specific signature genes. In FS, HGG, and MS, although the fibroblast cluster is comparable in abundance, distinct transcriptomic diversity has been noted. DEGs, high in FS and HGG fibroblasts compared to MS, were enriched for mitochondrial metabolic pathways. Such mitochondrial distribution and functional activity are required for tissue repair and regeneration around the injured site.[94–97] In the lungs, deficient mitochondrial function has been associated with fibrotic outcomes.[98,99]

We have previously reported that two-third of all fibroblasts in the granulation tissue of a skin wound are of myeloid origin.[20] Wound-site macrophages convert to fibroblast-like cells. Broadly, myeloid cells are well known for their robust intrinsic plasticity by virtue of which they may assume a wide array of cellular state and fate to enable physiological tissue repair and development.[100] Interestingly, compared to MS, abundance of the myeloid cell cluster was high in FS and HGG. Previous studies have shown that the metabolic cost of tissue repair is high and that under conditions of limited oxidative metabolism wounds acquire chronicity.[101] Comparable to the observation in fibroblasts, the myeloid cell cluster in FS and HGG were differentially enriched in mitochondrial genes. Several studies recognize active interplay between fibroblasts and myeloid cells in the repairing tissue.[12,20,102] In this work, CellChat analysis identified annexin signaling as a dominant pathway between myeloid cells and fibroblasts in FS and HGG tissues but not in MS tissue. Specifically, FPR1^{high} myeloid cells were identified as distinguishing kernel for FS and HGG relative to MS. FPR stimulation is known to bolster mitochondrial activity and related bioenergetics.[103,104] Our identification of FPR1 as a differentiating factor for myeloid cells of FS and HGG origin is consistent with a recent report on early-stage 10–17 weeks FS.[105] scRNA-seq analysis of fluorescence-activated cell sorting (FACS)-sorted cluster of differentiation (CD)45^{+} human FS cells identified the dominance of monocytes (LYZ^{high}/LYVE1^{low}/FPR1^{high}) and monocyte-macrophages (LYZ^{low}/LYVE1^{low}/FPR1^{high}) in early-stage FS (Table S12).[105] In this work, fetal macrophages appear as an abundant myeloid cell subcluster 4 and are characterized by FPR1^{high}. In these cells, the elevated expression levels of SPP1 and other fetal macrophage markers were noted. Pseudotime trajectory analysis assigned critical significance to this SPP1^{high} myeloid cell subpopulation as it marks the transition from FS to HGG tissues. The pseudotime trajectory originates from fetal macrophage subcluster 4 and extends to subcluster 0 representing HGG fibroblasts. The HGG fibroblasts at this pseudotime space were characterized by high expression level of *CCL2*. Also known as monocyte chemoattractant protein 1 (*MCP1*), CCL2 exhibits chemotactic activity for monocytes and basophils. It can also augment fetal macrophage function and physiological collagen deposition.[106,107] A significant role of CCL2 in achieving wound closure is well documented.[108–110] In summary, a comprehensive bioinformatic analysis of scRNA-seq data from human fetal and adult tissues identifies Annexin1-FPR1 signaling as a major communication pathway responsible for a functional relationship between myeloid cells and fibroblasts during tissue repair and regeneration.

Limitations of the study

Recognition of experimental limitations helps enhance rigor. First, the sample size for human FS scRNA-seq data was small (n = 3). This limitation was partly offset by the inclusion of related murine datasets. Second, this work was not powered to address sub-cellular compartments involved in tissue repair. The work relied on digital deconvolution of single-cell data and on cell subset markers. It is anticipated that this issue could eventually be resolved by exploring the signals at higher resolution using spatial transcriptomics and other imaging techniques. Third, the approach to characterize relevant ANXA1-FPR1 signaling in human FS was limited because of limited availability of human fetal tissue. The study of murine FS provides relevant data. Finally, this work will benefit from follow-up validation studies under experimental conditions that closely model the clinical conditions addressed.

STAR★METHODS

Detailed methods are provided in the online version of this paper and include the following:

- KEY RESOURCES TABLE
- RESOURCE AVAILABILITY
  - Lead contact
  - Materials availability
  - Data and code availability
- EXPERIMENTAL MODEL AND STUDY PARTICIPANT

SUPPLEMENTAL INFORMATION

Supplemental information can be found online at https://doi.org/10.1016/j.isci.2023.107533.

ACKNOWLEDGMENTS

We thank the members of the Sen lab at ICRME for actively participating in the discussion and constructive suggestions for completion of this study. We thank Leila N Fehme, Mohamad A Obeid, Simi Kaur, and Yashal D Butt for technical assistance.

Funding: This work was supported in part by the National Institute of Diabetes and Digestive and Kidney Diseases grants DK128845, DK135447, and DK125835 to CKS. This work was also supported in part by U.S. Department of Defense grants W81XWH-21-1-0033 to CKS and W81XWH-22-1-0146 to KS. This work was also supported in parts by NIH-R01 grant DK136814-01 to KS and NIH-K25 grant GM143572 to YX. Research programs led by CKS were supported by the Lilly Endowment INCITE (Indiana Collaborative Initiative for Talent Enrichment) program and John Templeton Foundation grant ID-61742.

AUTHOR CONTRIBUTIONS

RS, KS, and CKS designed the study. RS collected the dataset from public domain and implemented the available tools for single-cell data analysis with AA. YX participated in TNT chip development and testing. KS, MK, SK, SV, SM, MS, and SG participated in murine experiment and related data analysis. RS and KS wrote the manuscript. MK and CKS thoroughly reviewed and edited the manuscript. All authors read and approved the final manuscript.

DECLARATION OF INTERESTS

The authors declare no competing interests.

INCLUSION AND DIVERSITY

We support inclusive, diverse, and equitable conduct of research.

Received: June 8, 2022
Revised: June 6, 2023
Accepted: July 28, 2023
Published: August 2, 2023

REFERENCES

1. Ghatak, S., Chan, Y.C., Khanna, S., Banerjee, J., Weist, J., Roy, S., and Sen, C.K. (2015). Barrier Function of the Repaired Skin Is Disrupted Following Arrest of Dicer in Keratinocytes. Mol. Ther. *23*, 1201–1210. https://doi.org/10.1038/mt.2015.65.

2. Wikramanayake, T.C., Stojadinovic, O., and Tomic-Canic, M. (2014). Epidermal Differentiation in Barrier Maintenance and Wound Healing. Adv. Wound Care *3*, 272–280. https://doi.org/10.1089/wound.2013.0503.

3. Eming, S.A., Martin, P., and Tomic-Canic, M. (2014). Wound repair and regeneration: mechanisms, signaling, and translation. Sci. Transl. Med. *6*, 265sr6. https://doi.org/10.1126/scitranslmed.3009337.

4. Larouche, J., Sheoran, S., Maruyama, K., and Martino, M.M. (2018). Immune Regulation of Skin Wound Healing: Mechanisms and Novel Therapeutic Targets. Adv. Wound Care *7*, 209–231. https://doi.org/10.1089/wound.2017.0761.

5. Wilgus, T.A. (2007). Regenerative healing in fetal skin: a review of the literature. Ostomy. Wound. Manage. *53*, 16–31. quiz 32-13.

6. Willyard, C. (2018). Unlocking the secrets of scar-free skin healing. Nature *563*, S86–S88.

https://doi.org/10.1038/d41586-018-07430-w.

7. Monavarian, M., Kader, S., Moeinzadeh, S., and Jabbari, E. (2019). Regenerative Scar-Free Skin Wound Healing. Tissue Eng. Part B Rev. *25*, 294–311. https://doi.org/10.1089/ten.TEB.2018.0350.

8. Takeo, M., Lee, W., and Ito, M. (2015). Wound healing and skin regeneration. Cold Spring Harb. Perspect. Med. *5*, a023267. https://doi.org/10.1101/cshperspect.a023267.

9. Ghatak, S., Khanna, S., Roy, S., Thirunavukkarasu, M., Pradeep, S.R., Wulff, B.C., El Masry, M.S., Sharma, A., Palakurti, R., Ghosh, N., et al. (2023). Driving adult tissue repair via re-engagement of a pathway required for fetal healing. Mol. Ther. *31*, 454–470. https://doi.org/10.1016/j.ymthe.2022.09.002.

10. Schor, S.L., Ellis, I., Irwin, C.R., Banyard, J., Seneviratne, K., Dolman, C., Gilbert, A.D., and Chisholm, D.M. (1996). Subpopulations of fetal-like gingival fibroblasts: characterisation and potential significance for wound healing and the progression of periodontal disease. Oral Dis. *2*, 155–166. https://doi.org/10.1111/j.1601-0825.1996.tb00217.x.

11. Fournier, B.P.J., Larjava, H., and Häkkinen, L. (2013). Gingiva as a source of stem cells with therapeutic potential. Stem Cells Dev. *22*, 3157–3177. https://doi.org/10.1089/scd.2013.0015.

12. Guerrero-Juarez, C.F., Dedhia, P.H., Jin, S., Ruiz-Vega, R., Ma, D., Liu, Y., Yamaga, K., Shestova, O., Gay, D.L., Yang, Z., et al. (2019). Single-cell analysis reveals fibroblast heterogeneity and myeloid-derived adipocyte progenitors in murine skin wounds. Nat. Commun. *10*, 650. https://doi.org/10.1038/s41467-018-08247-x.

13. Plikus, M.V., Wang, X., Sinha, S., Forte, E., Thompson, S.M., Herzog, E.L., Driskell, R.R., Rosenthal, N., Biernaskie, J., and Horsley, V. (2021). Fibroblasts: Origins, definitions, and functions in health and disease. Cell *184*, 3852–3872. https://doi.org/10.1016/j.cell.2021.06.024.

14. Foster, D.S., Januszyk, M., Yost, K.E., Chinta, M.S., Gulati, G.S., Nguyen, A.T., Burcham, A.R., Salhotra, A., Ransom, R.C., Henn, D., et al. (2021). Integrated spatial multiomics reveals fibroblast fate during tissue repair. Proc. Natl. Acad. Sci. USA. *118*, e2110025118. https://doi.org/10.1073/pnas.2110025118.

15. Pal, D., Ghatak, S., Singh, K., Abouhashem, A.S., Kumar, M., El Masry, M.S., Mohanty, S.K., Palakurti, R., Rustagi, Y., Tabasum, S., et al. (2023). Identification of a physiologic vasculogenic fibroblast state to achieve tissue repair. Nat. Commun. *14*, 1129. https://doi.org/10.1038/s41467-023-36665-z.

16. Gharbia, F.Z., Abouhashem, A.S., Moqidem, Y.A., Elbaz, A.A., Abdellatif, A., Singh, K., Sen, C.K., and Azzazy, H.M.E. (2023). Adult skin fibroblast state change in murine wound healing. Sci. Rep. *13*, 886. https://doi.org/10.1038/s41598-022-27152-4.

17. Rognoni, E., Pisco, A.O., Hiratsuka, T., Sipilä, K.H., Belmonte, J.M., Mobasseri, S.A., Philippeos, C., Dilão, R., and Watt, F.M. (2018). Fibroblast state switching orchestrates dermal maturation and wound healing. Mol. Syst. Biol. *14*, e8174. https://doi.org/10.15252/msb.20178174.

18. Philippeos, C., Telerman, S.B., Oulès, B., Pisco, A.O., Shaw, T.J., Elgueta, R., Lombardi, G., Driskell, R.R., Soldin, M., Lynch, M.D., and Watt, F.M. (2018). Spatial and Single-Cell Transcriptional Profiling Identifies Functionally Distinct Human Dermal Fibroblast Subpopulations. J. Invest. Dermatol. *138*, 811–825. https://doi.org/10.1016/j.jid.2018.01.016.

19. Plikus, M.V., Guerrero-Juarez, C.F., Ito, M., Li, Y.R., Dedhia, P.H., Zheng, Y., Shao, M., Gay, D.L., Ramos, R., Hsi, T.C., et al. (2017). Regeneration of fat cells from myofibroblasts during wound healing. Science *355*, 748–752. https://doi.org/10.1126/science.aai8792.

20. Sinha, M., Sen, C.K., Singh, K., Das, A., Ghatak, S., Rhea, B., Blackstone, B., Powell, H.M., Khanna, S., and Roy, S. (2018). Direct conversion of injury-site myeloid cells to fibroblast-like cells of granulation tissue. Nat. Commun. *9*, 936. https://doi.org/10.1038/s41467-018-03208-w.

21. Mascharak, S., desJardins-Park, H.E., and Longaker, M.T. (2020). Fibroblast Heterogeneity in Wound Healing: Hurdles to Clinical Translation. Trends Mol. Med. *26*, 1101–1106. https://doi.org/10.1016/j.molmed.2020.07.008.

22. Rodrigues, M., Kosaric, N., Bonham, C.A., and Gurtner, G.C. (2019). Wound Healing: A Cellular Perspective. Physiol. Rev. *99*, 665–706. https://doi.org/10.1152/physrev.00067.2017.

23. Sen, C.K., and Roy, S. (2021). The Hyperglycemia Stranglehold Stifles Cutaneous EpithelialMesenchymal Plasticity and Functional Wound Closure. J. Invest. Dermatol. *141*, 1382–1385. https://doi.org/10.1016/j.jid.2020.11.021.

24. Singh, K., Sinha, M., Pal, D., Tabasum, S., Gnyawali, S.C., Khona, D., Sarkar, S., Mohanty, S.K., Soto-Gonzalez, F., Khanna, S., et al. (2019). Cutaneous Epithelial to Mesenchymal Transition Activator ZEB1 Regulates Wound Angiogenesis and Closure in a Glycemic Status-Dependent Manner. Diabetes *68*, 2175–2190. https://doi.org/10.2337/db19-0202.

25. Miscianinov, V., Martello, A., Rose, L., Parish, E., Cathcart, B., Mitić, T., Gray, G.A., Meloni, M., Al Haj Zen, A., and Caporali, A. (2018). MicroRNA-148b Targets the TGF-beta Pathway to Regulate Angiogenesis and Endothelial-to-Mesenchymal Transition during Skin Wound Healing. Mol. Ther. *26*, 1996–2007. https://doi.org/10.1016/j.ymthe.2018.05.002.

26. Singh, K., Rustagi, Y., Abouhashem, A.S., Tabasum, S., Verma, P., Hernandez, E., Pal, D., Khona, D.K., Mohanty, S.K., Kumar, M., et al. (2022). Genome-wide DNA hypermethylation opposes healing in patients with chronic wounds by impairing epithelial-mesenchymal transition. J. Clin. Invest. *132*, e157279. https://doi.org/10.1172/JCI157279.

27. Mascharak, S., desJardins-Park, H.E., Davitt, M.F., Griffin, M., Borrelli, M.R., Moore, A.L., Chen, K., Duoto, B., Chinta, M., Foster, D.S., et al. (2021). Preventing Engrailed-1 activation in fibroblasts yields wound regeneration without scarring. Science *372*, eaba2374. https://doi.org/10.1126/science.aba2374.

28. Leavitt, T., Hu, M.S., Borrelli, M.R., Januszyk, M., Garcia, J.T., Ransom, R.C., Mascharak, S., desJardins-Park, H.E., Litzenburger, U.M., Walmsley, G.G., et al. (2020). Prrx1 Fibroblasts Represent a Pro-fibrotic Lineage in the Mouse Ventral Dermis. Cell Rep. *33*, 108356. https://doi.org/10.1016/j.celrep.2020.108356.

29. Franzen, O., Gan, L.M., and Bjorkegren, J.L.M. (2019). PanglaoDB: a web server for exploration of mouse and human single-cell RNA sequencing data. Database *2019*, 1–9. https://doi.org/10.1093/database/baz046.

30. Muhl, L., Genové, G., Leptidis, S., Liu, J., He, L., Mocci, G., Sun, Y., Gustafsson, S., Buyandelger, B., Chivukula, I.V., et al. (2020). Single-cell analysis uncovers fibroblast heterogeneity and criteria for fibroblast and mural cell identification and discrimination. Nat. Commun. *11*, 3953. https://doi.org/10.1038/s41467-020-17740-1.

31. Ezure, T., Sugahara, M., and Amano, S. (2019). Senescent dermal fibroblasts negatively influence fibroblast extracellular matrix-related gene expression partly via secretion of complement factor D. Biofactors *45*, 556–562. https://doi.org/10.1002/biof.1512.

32. Rustagi, Y., Abouhashem, A.S., Verma, P., Verma, S.S., Hernandez, E., Liu, S., Kumar, M., Guda, P.R., Srivastava, R., Mohanty, S.K., et al. (2022). Endothelial Phospholipase Cgamma2 Improves Outcomes of Diabetic Ischemic Limb Rescue Following VEGF Therapy. Diabetes *71*, 1149–1165. https://doi.org/10.2337/db21-0830.

33. Deng, C.C., Hu, Y.F., Zhu, D.H., Cheng, Q., Gu, J.J., Feng, Q.L., Zhang, L.X., Xu, Y.P., Wang, D., Rong, Z., and Yang, B. (2021). Single-cell RNA-seq reveals fibroblast heterogeneity and increased mesenchymal fibroblasts in human fibrotic skin diseases. Nat. Commun. *12*, 3709. https://doi.org/10.1038/s41467-021-24110-y.

34. Szklarczyk, D., Gable, A.L., Nastou, K.C., Lyon, D., Kirsch, R., Pyysalo, S., Doncheva, N.T., Legeay, M., Fang, T., Bork, P., et al. (2021). The STRING database in 2021: customizable protein-protein networks, and functional characterization of user-uploaded gene/measurement sets. Nucleic Acids Res. *49*, D605–D612. https://doi.org/10.1093/nar/gkaa1074.

35. Szklarczyk, D., Gable, A.L., Lyon, D., Junge, A., Wyder, S., Huerta-Cepas, J., Simonovic,

M., Doncheva, N.T., Morris, J.H., Bork, P., et al. (2019). STRING v11: protein-protein association networks with increased coverage, supporting functional discovery in genome-wide experimental datasets. Nucleic Acids Res. *47*, D607–D613. https://doi.org/10.1093/nar/gky1131.

36. Solé-Boldo, L., Raddatz, G., Schütz, S., Mallm, J.P., Rippe, K., Lonsdorf, A.S., Rodríguez-Paredes, M., and Lyko, F. (2020). Single-cell transcriptomes of the human skin reveal age-related loss of fibroblast priming. Commun. Biol. *3*, 188. https://doi.org/10.1038/s42003-020-0922-4.

37. Kendall, R.T., and Feghali-Bostwick, C.A. (2014). Fibroblasts in fibrosis: novel roles and mediators. Front. Pharmacol. *5*, 123. https://doi.org/10.3389/fphar.2014.00123.

38. Makdissi, N., and Mass, E. (2021). Of myeloid cells and fibroblasts-A love story. Immunity *54*, 1371–1373. https://doi.org/10.1016/j.immuni.2021.06.016.

39. Jin, S., Guerrero-Juarez, C.F., Zhang, L., Chang, I., Ramos, R., Kuan, C.H., Myung, P., Plikus, M.V., and Nie, Q. (2021). Inference and analysis of cell-cell communication using CellChat. Nat. Commun. *12*, 1088. https://doi.org/10.1038/s41467-021-21246-9.

40. Han, P.F., Che, X.D., Li, H.Z., Gao, Y.Y., Wei, X.C., and Li, P.C. (2020). Annexin A1 involved in the regulation of inflammation and cell signaling pathways. Chin. J. Traumatol. *23*, 96–101. https://doi.org/10.1016/j.cjtee.2020.02.002.

41. Gobbetti, T., and Cooray, S.N. (2016). Annexin A1 and resolution of inflammation: tissue repairing properties and signalling signature. Biol. Chem. *397*, 981–993. https://doi.org/10.1515/hsz-2016-0200.

42. Leoni, G., and Nusrat, A. (2016). Annexin A1: shifting the balance towards resolution and repair. Biol. Chem. *397*, 971–979. https://doi.org/10.1515/hsz-2016-0180.

43. Leoni, G., Alam, A., Neumann, P.A., Lambeth, J.D., Cheng, G., McCoy, J., Hilgarth, R.S., Kundu, K., Murthy, N., Kusters, D., et al. (2013). Annexin A1, formyl peptide receptor, and NOX1 orchestrate epithelial repair. J. Clin. Invest. *123*, 443–454. https://doi.org/10.1172/JCI65831.

44. Liu, M., Chen, K., Yoshimura, T., Liu, Y., Gong, W., Le, Y., Gao, J.L., Zhao, J., Wang, J.M., and Wang, A. (2014). Formylpeptide receptors mediate rapid neutrophil mobilization to accelerate wound healing. PLoS One *9*, e90613. https://doi.org/10.1371/journal.pone.0090613.

45. Wang, G., Zhang, L., Chen, X., Xue, X., Guo, Q., Liu, M., and Zhao, J. (2016). Formylpeptide Receptors Promote the Migration and Differentiation of Rat Neural Stem Cells. Sci. Rep. *6*, 25946. https://doi.org/10.1038/srep25946.

46. Schneider, E.H., Weaver, J.D., Gaur, S.S., Tripathi, B.K., Jesaitis, A.J., Zelenka, P.S., Gao, J.L., and Murphy, P.M. (2012). The leukocyte chemotactic receptor FPR1 is functionally expressed on human lens epithelial cells. J. Biol. Chem. *287*, 40779–40792. https://doi.org/10.1074/jbc.M112.411181.

47. Wenceslau, C.F., McCarthy, C.G., Szasz, T., Calmasini, F.B., Mamenko, M., and Webb, R.C. (2019). Formyl peptide receptor-1 activation exerts a critical role for the dynamic plasticity of arteries via actin polymerization. Pharmacol. Res. *141*, 276–290. https://doi.org/10.1016/j.phrs.2019.01.015.

48. Xiao, W., Le, Q., Zhu, D., Dighe, A., Cui, Q., and Yang, X. (2021). Association of Fpr1 gene expression with osteogenesis and adipogenesis of adipose derived stem cells. Biochem. Biophys. Res. Commun. *574*, 33–38. https://doi.org/10.1016/j.bbrc.2021.08.044.

49. Marutani, T., Nishino, K., Miyaji, T., Kamada, K., Ohura, K., Kiso, Y., and Mukai, H. (2021). Mitocryptide-2: Identification of Its Minimum Structure for Specific Activation of FPR2-Possible Receptor Switching from FPR2 to FPR1 by Its Physiological C-terminal Cleavages. Int. J. Mol. Sci. *22*, 4084. https://doi.org/10.3390/ijms22084084.

50. Gallego-Perez, D., Pal, D., Ghatak, S., Malkoc, V., Higuita-Castro, N., Gnyawali, S., Chang, L., Liao, W.C., Shi, J., Sinha, M., et al. (2017). Topical tissue nano-transfection mediates non-viral stroma reprogramming and rescue. Nat. Nanotechnol. *12*, 974–979. https://doi.org/10.1038/nnano.2017.134.

51. Zhou, X., Brown, B.A., Siegel, A.P., El Masry, M.S., Zeng, X., Song, W., Das, A., Khandelwal, P., Clark, A., Singh, K., et al. (2020). Exosome-Mediated Crosstalk between Keratinocytes and Macrophages in Cutaneous Wound Healing. ACS Nano *14*, 12732–12748. https://doi.org/10.1021/acsnano.0c03064.

52. Xuan, Y., Ghatak, S., Clark, A., Li, Z., Khanna, S., Pak, D., Agarwal, M., Roy, S., Duda, P., and Sen, C.K. (2021). Fabrication and use of silicon hollow-needle arrays to achieve tissue nanotransfection in mouse tissue in vivo. Nat. Protoc. *16*, 5707–5738. https://doi.org/10.1038/s41596-021-00631-0.

53. Gordillo, G.M., Guda, P.R., Singh, K., Biswas, A., Abouhashem, A.S., Rustagi, Y., Sen, A., Kumar, M., Das, A., Ghatak, S., et al. (2023). Tissue nanotransfection causes tumor regression by its effect on nanovesicle cargo that alters microenvironmental macrophage state. Mol. Ther. *31*, 1402–1417. https://doi.org/10.1016/j.ymthe.2022.11.003.

54. Coolen, N.A., Schouten, K.C.W.M., Middelkoop, E., and Ulrich, M.M.W. (2010). Comparison between human fetal and adult skin. Arch. Dermatol. Res. *302*, 47–55. https://doi.org/10.1007/s00403-009-0989-8.

55. Morabito, S., Miyoshi, E., Michael, N., Shahin, S., Martini, A.C., Head, E., Silva, J., Leavy, K., Perez-Rosendahl, M., and Swarup, V. (2021). Single-nucleus chromatin accessibility and transcriptomic characterization of Alzheimer's disease. Nat. Genet. *53*, 1143–1155. https://doi.org/10.1038/s41588-021-00894-z.

56. Morabito, S., Reese, F., Rahimzadeh, N., Miyoshi, E., and Swarup, V. (2022). High dimensional co-expression networks enable discovery of transcriptomic drivers in complex biological systems. Preprint at bioRxiv, https://doi.org/10.1101/2022.09.22.509094.

57. Van de Sande, B., Flerin, C., Davie, K., De Waegeneer, M., Hulselmans, G., Aibar, S., Seurinck, R., Saelens, W., Cannoodt, R., Rouchon, Q., et al. (2020). A scalable SCENIC workflow for single-cell gene regulatory network analysis. Nat. Protoc. *15*, 2247–2276. https://doi.org/10.1038/s41596-020-0336-2.

58. Eraslan, G., Drokhlyansky, E., Anand, S., Fiskin, E., Subramanian, A., Slyper, M., Wang, J., Van Wittenberghe, N., Rouhana, J.M., Waldman, J., et al. (2022). Single-nucleus cross-tissue molecular reference maps toward understanding disease gene function. Science *376*, eabl4290. https://doi.org/10.1126/science.abl4290.

59. Cheng, S., Li, Z., Gao, R., Xing, B., Gao, Y., Yang, Y., Qin, S., Zhang, L., Ouyang, H., Du, P., et al. (2021). A pan-cancer single-cell transcriptional atlas of tumor infiltrating myeloid cells. Cell *184*, 792–809.e23. https://doi.org/10.1016/j.cell.2021.01.010.

60. Buechler, M.B., Pradhan, R.N., Krishnamurty, A.T., Cox, C., Calviello, A.K., Wang, A.W., Yang, Y.A., Tam, L., Caothien, R., Roose-Girma, M., et al. (2021). Cross-tissue organization of the fibroblast lineage. Nature *593*, 575–579. https://doi.org/10.1038/s41586-021-03549-5.

61. Xue, D., Tabib, T., Morse, C., and Lafyatis, R. (2020). Transcriptome landscape of myeloid cells in human skin reveals diversity, rare populations and putative DC progenitors. J. Dermatol. Sci. *97*, 41–49. https://doi.org/10.1016/j.jdermsci.2019.11.012.

62. Suryawanshi, H., Morozov, P., Straus, A., Sahasrabudhe, N., Max, K.E.A., Garzia, A., Kustagi, M., Tuschl, T., and Williams, Z. (2018). A single-cell survey of the human first-trimester placenta and decidua. Sci. Adv. *4*, eaau4788. https://doi.org/10.1126/sciadv.aau4788.

63. Alexaki, V.I., Simantiraki, D., Panayiotopoulou, M., Rasouli, O., Venihaki, M., Castana, O., Alexakis, D., Kampa, M., Stathopoulos, E.N., and Castanas, E. (2012). Adipose tissue-derived mesenchymal cells support skin reepithelialization through secretion of KGF-1 and PDGF-BB: comparison with dermal fibroblasts. Cell Transplant. *21*, 2441–2454. https://doi.org/10.3727/096368912X637064.

64. Barker, J.C., Barker, A.D., Bills, J., Huang, J., Wight-Carter, M., Delgado, I., Noble, D.L., Huang, L.J., Porteus, M.H., and Davis, K.E. (2014). Genome editing of mouse fibroblasts by homologous recombination for sustained secretion of PDGF-B and augmentation of wound healing. Plast. Reconstr. Surg. *134*, 389e–401e. https://doi.org/10.1097/PRS.0000000000000427.

65. Chen, L., Wang, Z., Li, S., Zhao, G., Tian, M., and Sun, Z. (2012). SFRP2 and slug

contribute to cellular resistance to apoptosis in hypertrophic scars. PLoS One *7*, e50229. https://doi.org/10.1371/journal.pone.0050229.

66. Shi, J., Xiao, H., Li, J., Zhang, J., Li, Y., Zhang, J., Wang, X., Bai, X., Tao, K., Hu, D., and Guan, H. (2018). Wild-type p53-modulated autophagy and autophagic fibroblast apoptosis inhibit hypertrophic scar formation. Lab. Invest. *98*, 1423–1437. https://doi.org/10.1038/s41374-018-0099-3.

67. Simon, F., Bergeron, D., Larochelle, S., Lopez-Vallé, C.A., Genest, H., Armour, A., and Moulin, V.J. (2012). Enhanced secretion of TIMP-1 by human hypertrophic scar keratinocytes could contribute to fibrosis. Burns *38*, 421–427. https://doi.org/10.1016/j.burns.2011.09.001.

68. Branski, L.K., Pereira, C.T., Herndon, D.N., and Jeschke, M.G. (2007). Gene therapy in wound healing: present status and future directions. Gene Ther. *14*, 1–10. https://doi.org/10.1038/sj.gt.3302837.

69. Tanriverdi-Akhisaroglu, S., Menderes, A., and Oktay, G. (2009). Matrix metalloproteinase-2 and -9 activities in human keloids, hypertrophic and atrophic scars: a pilot study. Cell Biochem. Funct. *27*, 81–87. https://doi.org/10.1002/cbf.1537.

70. Shi, G., Zhang, Z., Friesen, T.L., Bansal, U., Cloutier, S., Wicker, T., Rasmussen, J.B., and Faris, J.D. (2016). Marker development, saturation mapping, and high-resolution mapping of the Septoria nodorum blotch susceptibility gene Snn3-B1 in wheat. Mol. Genet. Genomics. *291*, 107–119. https://doi.org/10.1007/s00438-015-1091-x.

71. Ogawa, R., Watanabe, A., Than Naing, B., Sasaki, M., Fujita, A., Akaishi, S., Hyakusoku, H., and Shimada, T. (2014). Associations between keloid severity and single-nucleotide polymorphisms: importance of rs8032158 as a biomarker of keloid severity. J. Invest. Dermatol. *134*, 2041–2043. https://doi.org/10.1038/jid.2014.71.

72. Balaji, S., LeSaint, M., Bhattacharya, S.S., Moles, C., Dhamija, Y., Kidd, M., Le, L.D., King, A., Shaaban, A., Crombleholme, T.M., et al. (2014). Adenoviral-mediated gene transfer of insulin-like growth factor 1 enhances wound healing and induces angiogenesis. J. Surg. Res. *190*, 367–377. https://doi.org/10.1016/j.jss.2014.02.051.

73. Hu, Z.C., Tang, B., Guo, D., Zhang, J., Liang, Y.Y., Ma, D., and Zhu, J.Y. (2014). Expression of insulin-like growth factor-1 receptor in keloid and hypertrophic scar. Clin. Exp. Dermatol. *39*, 822–828. https://doi.org/10.1111/ced.12407.

74. Liu, X., Ma, L., Liang, J., Zhang, B., Teng, J., and Gao, C. (2013). RNAi functionalized collagen-chitosan/silicone membrane bilayer dermal equivalent for full-thickness skin regeneration with inhibited scarring. Biomaterials *34*, 2038–2048. https://doi.org/10.1016/j.biomaterials.2012.11.062.

75. Lee, D.E., Trowbridge, R.M., Ayoub, N.T., and Agrawal, D.K. (2015). High-mobility Group Box Protein-1, Matrix Metalloproteinases, and Vitamin D in Keloids and Hypertrophic Scars. Plast. Reconstr. Surg. Glob. Open *3*, e425. https://doi.org/10.1097/GOX.0000000000000391.

76. Xue, M., and Jackson, C.J. (2015). Extracellular Matrix Reorganization During Wound Healing and Its Impact on Abnormal Scarring. Adv. Wound Care *4*, 119–136. https://doi.org/10.1089/wound.2013.0485.

77. Finnson, K.W., McLean, S., Di Guglielmo, G.M., and Philip, A. (2013). Dynamics of Transforming Growth Factor Beta Signaling in Wound Healing and Scarring. Adv. Wound Care *2*, 195–214. https://doi.org/10.1089/wound.2013.0429.

78. Johnson, K.E., and Wilgus, T.A. (2014). Vascular Endothelial Growth Factor and Angiogenesis in the Regulation of Cutaneous Wound Repair. Adv. Wound Care *3*, 647–661. https://doi.org/10.1089/wound.2013.0517.

79. Cao, J., Spielmann, M., Qiu, X., Huang, X., Ibrahim, D.M., Hill, A.J., Zhang, F., Mundlos, S., Christiansen, L., Steemers, F.J., et al. (2019). The single-cell transcriptional landscape of mammalian organogenesis. Nature *566*, 496–502. https://doi.org/10.1038/s41586-019-0969-x.

80. Bullard, K.M., Longaker, M.T., and Lorenz, H.P. (2003). Fetal wound healing: current biology. World J. Surg. *27*, 54–61. https://doi.org/10.1007/s00268-002-6737-2.

81. Cho, Y.D., Kim, K.H., Lee, Y.M., Ku, Y., and Seol, Y.J. (2021). Periodontal Wound Healing and Tissue Regeneration: A Narrative Review. Pharmaceuticals *14*, 456. https://doi.org/10.3390/ph14050456.

82. Ahangar, P., Mills, S.J., Smith, L.E., Gronthos, S., and Cowin, A.J. (2020). Human gingival fibroblast secretome accelerates wound healing through anti-inflammatory and pro-angiogenic mechanisms. NPJ Regen. Med. *5*, 24. https://doi.org/10.1038/s41536-020-00109-9.

83. Griffin, M.F., desJardins-Park, H.E., Mascharak, S., Borrelli, M.R., and Longaker, M.T. (2020). Understanding the impact of fibroblast heterogeneity on skin fibrosis. Dis. Model. Mech. *13*, dmm044164. https://doi.org/10.1242/dmm.044164.

84. Rinkevich, Y., Walmsley, G.G., Hu, M.S., Maan, Z.N., Newman, A.M., Drukker, M., Januszyk, M., Krampitz, G.W., Gurtner, G.C., Lorenz, H.P., et al. (2015). Skin fibrosis. Identification and isolation of a dermal lineage with intrinsic fibrogenic potential. Science *348*, aaa2151. https://doi.org/10.1126/science.aaa2151.

85. Driskell, R.R., Lichtenberger, B.M., Hoste, E., Kretzschmar, K., Simons, B.D., Charalambous, M., Ferron, S.R., Herault, Y., Pavlovic, G., Ferguson-Smith, A.C., and Watt, F.M. (2013). Distinct fibroblast lineages determine dermal architecture in skin development and repair. Nature *504*, 277–281. https://doi.org/10.1038/nature12783.

86. Vorstandlechner, V., Laggner, M., Kalinina, P., Haslik, W., Radtke, C., Shaw, L., Lichtenberger, B.M., Tschachler, E., Ankersmit, H.J., and Mildner, M. (2020). Deciphering the functional heterogeneity of skin fibroblasts using single-cell RNA sequencing. Faseb. J. *34*, 3677–3692. https://doi.org/10.1096/fj.201902001RR.

87. He, H., Suryawanshi, H., Morozov, P., Gay-Mimbrera, J., Del Duca, E., Kim, H.J., Kameyama, N., Estrada, Y., Der, E., Krueger, J.G., et al. (2020). Single-cell transcriptome analysis of human skin identifies novel fibroblast subpopulation and enrichment of immune subsets in atopic dermatitis. J. Allergy Clin. Immunol. *145*, 1615–1628. https://doi.org/10.1016/j.jaci.2020.01.042.

88. Lin, R.Y., and Adzick, N.S. (1996). The role of the fetal fibroblast and transforming growth factor-beta in a model of human fetal wound repair. Semin. Pediatr. Surg. *5*, 165–174.

89. Guo, F., Carter, D.E., Mukhopadhyay, A., and Leask, A. (2011). Gingival fibroblasts display reduced adhesion and spreading on extracellular matrix: a possible basis for scarless tissue repair? PLoS One *6*, e27097. https://doi.org/10.1371/journal.pone.0027097.

90. Larjava, H., Wiebe, C., Gallant-Behm, C., Hart, D.A., Heino, J., and Häkkinen, L. (2011). Exploring scarless healing of oral soft tissues. J. Can. Dent. Assoc. *77*, b18.

91. Mah, W., Jiang, G., Olver, D., Cheung, G., Kim, B., Larjava, H., and Häkkinen, L. (2014). Human gingival fibroblasts display a non-fibrotic phenotype distinct from skin fibroblasts in three-dimensional cultures. PLoS One *9*, e90715. https://doi.org/10.1371/journal.pone.0090715.

92. Mak, K., Manji, A., Gallant-Behm, C., Wiebe, C., Hart, D.A., Larjava, H., and Häkkinen, L. (2009). Scarless healing of oral mucosa is characterized by faster resolution of inflammation and control of myofibroblast action compared to skin wounds in the red Duroc pig model. J. Dermatol. Sci. *56*, 168–180. https://doi.org/10.1016/j.jdermsci.2009.09.005.

93. Egusa, H., Okita, K., Kayashima, H., Yu, G., Fukuyasu, S., Saeki, M., Matsumoto, T., Yamanaka, S., and Yatani, H. (2010). Gingival fibroblasts as a promising source of induced pluripotent stem cells. PLoS One *5*, e12743. https://doi.org/10.1371/journal.pone.0012743.

94. Madan, S., Uttekar, B., Chowdhary, S., and Rikhy, R. (2021). Mitochondria Lead the Way: Mitochondrial Dynamics and Function in Cellular Movements in Development and Disease. Front. Cell Dev. Biol. *9*, 781933. https://doi.org/10.3389/fcell.2021.781933.

95. Banerjee, A., Lindenmair, A., Hennerbichler, S., Steindorf, P., Steinborn, R., Kozlov, A.V., Redl, H., Wolbank, S., and Weidinger, A. (2018). Cellular and Site-Specific Mitochondrial Characterization of Vital Human Amniotic Membrane. Cell Transplant. *27*, 3–11. https://doi.org/10.1177/0963689717735332.

96. Balcázar, M., Cañizares, S., Borja, T., Pontón, P., Bisiou, S., Carabasse, E., Bacilieri, A., Canavese, C., Diaz, R.F., Cabrera, F., and Caicedo, A. (2020). Bases for Treating Skin Aging With Artificial Mitochondrial Transfer/Transplant (AMT/T). Front. Bioeng. Biotechnol. *8*, 919. https://doi.org/10.3389/fbioe.2020.00919.

97. Ko, S.H., Choi, G.E., Oh, J.Y., Lee, H.J., Kim, J.S., Chae, C.W., Choi, D., and Han, H.J. (2018). Author Correction: Succinate promotes stem cell migration through the GPR91-dependent regulation of DRP1-mediated mitochondrial fission. Sci. Rep. *8*, 13326. https://doi.org/10.1038/s41598-018-31586-0.

98. Larson-Casey, J.L., He, C., and Carter, A.B. (2020). Mitochondrial quality control in pulmonary fibrosis. Redox Biol. *33*, 101426. https://doi.org/10.1016/j.redox.2020.101426.

99. Li, X., Zhang, W., Cao, Q., Wang, Z., Zhao, M., Xu, L., and Zhuang, Q. (2020). Mitochondrial dysfunction in fibrotic diseases. Cell Death Discov. *6*, 80. https://doi.org/10.1038/s41420-020-00316-9.

100. Sun, Y., Kaur, K., Kanayama, K., Morinaga, K., Park, S., Hokugo, A., Kozlowska, A., McBride, W.H., Li, J., Jewett, A., and Nishimura, I. (2016). Plasticity of Myeloid Cells during Oral Barrier Wound Healing and the Development of Bisphosphonate-related Osteonecrosis of the Jaw. J. Biol. Chem. *291*, 20602–20616. https://doi.org/10.1074/jbc.M116.735795.

101. Cano Sanchez, M., Lancel, S., Boulanger, E., and Neviere, R. (2018). Targeting Oxidative Stress and Mitochondrial Dysfunction in the Treatment of Impaired Wound Healing: A Systematic Review. Antioxidants *7*, 98. https://doi.org/10.3390/antiox7080098.

102. Mescher, A.L. (2017). Macrophages and fibroblasts during inflammation and tissue repair in models of organ regeneration. Regeneration (Oxf) *4*, 39–53. https://doi.org/10.1002/reg2.77.

103. Bao, Y., Ledderose, C., Seier, T., Graf, A.F., Brix, B., Chong, E., and Junger, W.G. (2014). Mitochondria regulate neutrophil activation by generating ATP for autocrine purinergic signaling. J. Biol. Chem. *289*, 26794–26803. https://doi.org/10.1074/jbc.M114.572495.

104. Bao, Y., Ledderose, C., Graf, A.F., Brix, B., Birsak, T., Lee, A., Zhang, J., and Junger, W.G. (2015). mTOR and differential activation of mitochondria orchestrate neutrophil chemotaxis. J. Cell Biol. *210*, 1153–1164. https://doi.org/10.1083/jcb.201503066.

105. Xu, Y., Zhang, J., Hu, Y., Li, X., Sun, L., Peng, Y., Sun, Y., Liu, B., Bian, Z., and Rong, Z. (2021). Single-cell transcriptome analysis reveals the dynamics of human immune cells during early fetal skin development. Cell Rep. *36*, 109524. https://doi.org/10.1016/j.celrep.2021.109524.

106. Castela, M., Nassar, D., Sbeih, M., Jachiet, M., Wang, Z., and Aractingi, S. (2017). Ccl2/Ccr2 signalling recruits a distinct fetal microchimeric population that rescues delayed maternal wound healing. Nat. Commun. *8*, 15463. https://doi.org/10.1038/ncomms15463.

107. Jürgensen, H.J., Silva, L.M., Krigslund, O., van Putten, S., Madsen, D.H., Behrendt, N., Engelholm, L.H., and Bugge, T.H. (2019). CCL2/MCP-1 signaling drives extracellular matrix turnover by diverse macrophage subsets. Matrix Biol. *1*, 100003. https://doi.org/10.1016/j.mbplus.2019.03.002.

108. Lu, H., Huang, D., Ransohoff, R.M., and Zhou, L. (2011). Acute skeletal muscle injury: CCL2 expression by both monocytes and injured muscle is required for repair. Faseb. J. *25*, 3344–3355. https://doi.org/10.1096/fj.10-178939.

109. Lee, B.C., Song, J., Lee, A., Cho, D., and Kim, T.S. (2020). Erythroid differentiation regulator 1 promotes wound healing by inducing the production of CC motif chemokine ligand 2 via the activation of MAP kinases in vitro and in vivo. Int. J. Mol. Med. *46*, 2185–2193. https://doi.org/10.3892/ijmm.2020.4762.

110. Jablonski, C.L., Leonard, C., Salo, P., and Krawetz, R.J. (2019). CCL2 But Not CCR2 Is Required for Spontaneous Articular Cartilage Regeneration Post-Injury. J. Orthop. Res. *37*, 2561–2574. https://doi.org/10.1002/jor.24444.

111. Reitermaier, R., Krausgruber, T., Fortelny, N., Ayub, T., Vieyra-Garcia, P.A., Kienzl, P., Wolf, P., Scharrer, A., Fiala, C., Kölz, M., et al. (2021). alphabetagammadelta T cells play a vital role in fetal human skin development and immunity. J. Exp. Med. *218*, e20201189. https://doi.org/10.1084/jem.20201189.

112. Williams, D.W., Greenwell-Wild, T., Brenchley, L., Dutzan, N., Overmiller, A., Sawaya, A.P., Webb, S., Martin, D., NIDCD/NIDCR Genomics and Computational Biology Core, , et al.Hajishengallis, G. (2021). Human oral mucosa cell atlas reveals a stromal-neutrophil axis regulating tissue immunity. Cell *184*, 4090–4104.e15. https://doi.org/10.1016/j.cell.2021.05.013.

113. Rojahn, T.B., Vorstandlechner, V., Krausgruber, T., Bauer, W.M., Alkon, N., Bangert, C., Thaler, F.M., Sadeghyar, F., Fortelny, N., Gernedl, V., et al. (2020). Single-cell transcriptomics combined with interstitial fluid proteomics defines cell type-specific immune regulation in atopic dermatitis. J. Allergy Clin. Immunol. *146*, 1056–1069. https://doi.org/10.1016/j.jaci.2020.03.041.

114. Wang, A., Rahman, N.T., McGeary, M.K., Murphy, M., McHenry, A., Peterson, D., Bosenberg, M., Flavell, R.A., King, B., and Damsky, W. (2021). Treatment of granuloma annulare and suppression of proinflammatory cytokine activity with tofacitinib. J. Allergy Clin. Immunol. *147*, 1795–1809. https://doi.org/10.1016/j.jaci.2020.10.012.

115. Gaydosik, A.M., Queen, D.S., Trager, M.H., Akilov, O.E., Geskin, L.J., and Fuschiotti, P. (2020). Genome-wide transcriptome analysis of the STAT6-regulated genes in advanced-stage cutaneous T-cell lymphoma. Blood *136*, 1748–1759. https://doi.org/10.1182/blood.2019004725.

116. Butler, A., Hoffman, P., Smibert, P., Papalexi, E., and Satija, R. (2018). Integrating single-cell transcriptomic data across different conditions, technologies, and species. Nat. Biotechnol. *36*, 411–420. https://doi.org/10.1038/nbt.4096.

117. Abouhashem, A.S., Singh, K., Azzazy, H.M.E., and Sen, C.K. (2020). Is Low Alveolar Type II Cell SOD3 in the Lungs of Elderly Linked to the Observed Severity of COVID-19? Antioxid. Redox Signal. *33*, 59–65. https://doi.org/10.1089/ars.2020.8111.

118. Hafemeister, C., and Satija, R. (2019). Normalization and variance stabilization of single-cell RNA-seq data using regularized negative binomial regression. Genome Biol. *20*, 296. https://doi.org/10.1186/s13059-019-1874-1.

119. Shannon, P., Markiel, A., Ozier, O., Baliga, N.S., Wang, J.T., Ramage, D., Amin, N., Schwikowski, B., and Ideker, T. (2003). Cytoscape: a software environment for integrated models of biomolecular interaction networks. Genome Res. *13*, 2498–2504. https://doi.org/10.1101/gr.1239303.

120. Trapnell, C., Cacchiarelli, D., Grimsby, J., Pokharel, P., Li, S., Morse, M., Lennon, N.J., Livak, K.J., Mikkelsen, T.S., and Rinn, J.L. (2014). The dynamics and regulators of cell fate decisions are revealed by pseudotemporal ordering of single cells. Nat. Biotechnol. *32*, 381–386. https://doi.org/10.1038/nbt.2859.

121. Parra-Hernández, R.M., Posada-Quintero, J.I., Acevedo-Charry, O., and Posada-Quintero, H.F. (2020). Uniform Manifold Approximation and Projection for Clustering Taxa through Vocalizations in a Neotropical Passerine (Rough-Legged Tyrannulet, Phyllomyias burmeisteri). Animals. *10*, 1406. https://doi.org/10.3390/ani10081406.

122. Sarkar, J., Luo, Y., Zhou, Q., Ivakhnitskaia, E., Lara, D., Katz, E., Sun, M.G., Guaiquil, V., and Rosenblatt, M. (2022). VEGF receptor heterodimers and homodimers are differentially expressed in neuronal and endothelial cell types. PLoS One *17*, e0269818. https://doi.org/10.1371/journal.pone.0269818.

123. Singh, K., Pal, D., Sinha, M., Ghatak, S., Gnyawali, S.C., Khanna, S., Roy, S., and Sen, C.K. (2017). Epigenetic Modification of MicroRNA-200b Contributes to Diabetic Vasculopathy. Mol. Ther. *25*, 2689–2704. https://doi.org/10.1016/j.ymthe.2017.09.009.

STAR★METHODS

KEY RESOURCES TABLE

REAGENT or RESOURCE	SOURCE	IDENTIFIER
Antibodies		
Mouse monoclonal anti-Annexin A1(ANXA1)	MYBIOSOURCE	Cat#MBS7612792 RRID: N/A
Rabbit polyclonal anti-FPR1	Novus biologicals	Cat#NBP2-47452 RRID: N/A
Duolink *In Situ* PLA Probe Anti-Rabbit PLUS	Sigma-Aldrich	Cat# DUO92002, RRID: AB_2810940)
Duolink *In Situ* PLA Probe Anti-Mouse MINUS Antibody	Sigma-Aldrich	Cat# DUO92004, RRID: AB_2713942
Biological samples		
C57BL6 skin and gingiva samples	The Jackson Laboratory	RRID: IMSR_JAX:000664
Chemicals, peptides, and recombinant proteins		
Duolink® *In Situ* Wash Buffers, Fluorescence	Sigma-Aldrich	DUO82049
Duolink® *In Situ* Detection Reagents Red	Sigma-Aldrich	DUO92008
Duolink® *In Situ* Mounting Medium with DAPI	Sigma-Aldrich	DUO82040
Experimental models: Organisms/strains		
C57BL6	The Jackson Laboratory	RRID: IMSR_JAX:000664
Recombinant DNA		
FPR1 ORF(NM_013521)	NovoPro labs	Cat.#: 749474-1
Data source		
Reitermaier et al.'s raw and processed scRNA-seq data	Reitermaier et al.[111]	GSE156972
Williams et al.'s raw and processed scRNA-seq data	Williams et al.[112]	GSE164241
Rojahn et al.'s raw and processed scRNA-seq data	Rojahn et al.[113]	GSE153760
Rustagi et al.'s raw and processed scRNA-seq data	Rustagi et al.[32]	GSE182208
Wang et al.'s raw and processed scRNA-seq data	Wang et al.[114]	GSE158924
Gaydosik et al.'s raw and processed scRNA-seq data	Gaydosik et al.[115]	GSE147944
Singh et al.'s raw and processed scRNA-seq data	Singh et al.[26]	GSE176415
Software and algorithms		
ImageJ	Schneider et al.,[46] Nature Methods	https://imagej.nih.gov/ij/
Zen software	Zeiss microscopy	https://www.zeiss.com/microscopy/en/products/software/zeiss-zen-lite.html
Seurat	https://satijalab.org/seurat/index.html	Version 4.0.2
SingleCellExperiment	https://bioconductor.org/packages/release/bioc/html/SingleCellExperiment.html	Version 3.17
dplyr	https://cran.r-project.org/web/packages/dplyr/index.html	Version 1.1.2

(*Continued on next page*)

Continued

REAGENT or RESOURCE	SOURCE	IDENTIFIER
Matrix	https://cran.r-project.org/web/packages/Matrix/index.html	Version 1.6–0
ggplot2	https://cran.r-project.org/web/packages/ggplot2/index.html	Version 3.4.2
hdf5r	https://cran.r-project.org/web/packages/hdf5r/index.html	Version 1.3.8
tidyverse	https://cran.r-project.org/web/packages/tidyverse/index.html	Version 2.0
sctransform	https://cran.r-project.org/web/packages/sctransform/index.html	Version 0.3.5
CellChat	https://github.com/sqjin/CellChat	Version 1.1.0
Monocle3	https://cole-trapnell-lab.github.io/monocle3/	Version 1.2.9
patchwork	https://cran.r-project.org/web/packages/patchwork/index.html	Version 1.1.2
hdWGCNA	https://smorabit.github.io/hdWGCNA/index.html	Version 0.2.19
cowplot	https://cran.r-project.org/web/packages/cowplot/index.html	Version 1.1.1
WGCNA	https://cran.r-project.org/web/packages/WGCNA/index.html	Version 1.72–1
Harmony	https://cran.r-project.org/web/packages/harmony/index.html	Version 0.1.1
SCENIC	https://github.com/aertslab/SCENIC	Version 1.2.4
Others		
Zeiss Axio Scan fluorescence microscope	Zeiss microscopy	https://www.zeiss.com/microscopy/en/products/imaging-systems/axioscan-for-biology.html

RESOURCE AVAILABILITY

Lead contact

Additional information and requests for resources and reagents should be directed to and will be completed by the lead contact, Chandan K. Sen (cksen@iu.edu; c.k.sen@pitt.edu).

Materials availability

This study did not generate any new raw data or unique reagents.

Data and code availability

- Data reported in this paper will be shared by the lead contact upon request.
- Source codes for entire data analysis are accessible via github link below: https://github.com/RajneeshSrivastava/scRNA-skin-tissue-repair.
- Any additional information required to reanalyze the data reported in this paper is available from the lead contact upon request.

EXPERIMENTAL MODEL AND STUDY PARTICIPANT

Animal model

For fetal (E15.5) skin collection, two E10 timed plug C57BL6 female mice (age 8 weeks) and age matched two male mice were purchased from the Jackson Laboratory, Bar Harbor, ME. On E15.5 the pregnant

females were euthanized by CO_2 asphyxiation and embryos were removed to collect the fetal skin. Additionally, adult dorsal skin and gingival tissues were harvested from the parent females and adult males as mentioned above. For wounding experiments, C57BL6 mice (male, 8-week-old) were purchased from the Jackson Laboratory. All animal experiments were conducted in accordance with the US National Institutes of Health Guide for the Care and Use of Laboratory Animals and approved by the Institutional Animal Care and Use Committee of Indiana University School of Medicine.

METHOD DETAILS

Data collection and processing

Single-cell RNA-seq data of healthy human fetal skin (FS),[111] gingiva (HGG)[112] and mature skin (MS)[32,113–115] were downloaded from multiple studies as documented in Table S1. Processed data available in.h5 or in split formats viz. barcodes.tsv.gz, matrix.mtx.gz, features.tsv.gz were used in this study. We employed Seurat[32,116,117] (package in R) for integration and analysis of collected dataset. Briefly, we created Seurat objects for all the processed scRNA-seq dataset with cutoffs for min.cells = 3 and min.features = 200. Further, we computed the percent mitochondrial genes to ensure the 15% limit on cells with high mitochondrial RNA. Quality filtering and normalization of each Seurat object was done using 'SCT-transformation'[118] module in Seurat. These normalized Seurat objects were integrated using canonical correlation analysis (CCA) method in Seurat. Further, clustering analysis was performed with resolution 0.25. Resulting cluster of cells were shown in tSNE plot and the proportion of cells per tissue type were calculated. Also, cluster specific markers were identified using 'FindAllMarkers' module in Seurat and parsed onto PanglaoDb[29] to assign the cell types.

Differential expression and function enrichment analysis of fibroblast cluster

Fibroblast cluster was isolated from all the clusters using 'subset' module in Seurat. Differential expression analysis between FS and MS fibroblast was performed using 'FindMarkers' module in Seurat with $\log_2$ fold change threshold = 0.3, min.pct = 0.30 cutoffs and other default parameters. Wilcoxon rank-sum test was used for significant testing. Genes, that were significantly high in FS fibroblast compared to MS-Fibroblast at q-value $\leq$0.01 were analyzed for gene-gene association and function enrichment using STRING[34] database. Obtained gene association network was customized in Cytoscape[119] to show the genes enriched for major GO processes.

Cell-cell interactome analysis

Cells communicate with each other to provide the cellular identity. To investigate the cellular communication among the obtained clusters of cells in FS HGG and MS samples, we employed CellChat[39] package in R. Briefly, the obtained cell clusters (Seurat objects) were subset for FS, HGG and MS groups. Further, CellChat object for each group was created using 'createCellChat' module of CellChat package in R. For each CellChat object, the total interactions were computed and differential interactome between each pair of groups were visualized using 'netVisual_diffInteraction' module of CellChat. Relative information flow of the connectome for each group was investigated using 'rankNet' module and the signaling pathways contributed by these interactions were visualized as stacked proportional barplot. Also, the aggregated incoming and outgoing patterns for signaling pathways identified in each group's connectome across the original clusters was visualized as heatmap.

Comparison of the fibroblast and myeloid cell clusters and re-clustering analysis

We isolated the fibroblast and myeloid clusters from the original cluster of cells using 'subset' module in Seurat. Differential expression analysis for comparisons i.e., FS vs. MS and HGG vs. MS was performed as described previously and for both, fibroblast and myeloid cells separately. Differentially expressed genes for each tested group were compared using venn diagram. Also, the common gene pool obtained from each test were compared across fibroblast and myeloid clusters. Expression profile of common genes upregulated in both FS and HGG with respect to MS were illustrated in violin plots. These combined cell types were re-clustered using 'RunPCA' followed by 'FindNeighbors', 'RunTSNE' and 'FindClusters' (at resolution = 0.25) modules in Seurat. Obtained subclusters were visualized in tSNE plot.

Construction of co-expression modules using single cell data of fibroblast and myeloid cells

High dimensional scRNA data of isolated fibroblast and myeloid cells were used to construct the gene expression modules using hdWGCNA.[55,56] This tool employed bootstrapped aggregation (K-nearest neighbors (KNN algorithm) to construct metacell, representing the aggregated transcriptomic profile

from these datasets. "TestSoftPowers" function was utilized to inspect a soft power threshold for appropriate network topology of co-expression network. Further, gene-gene correlation network was constructed using "ConstructNetwork" function in hdWGCNA. A distinct network structures and sets of gene modules was thus established and an unsupervised hierarchically clustered dendogram was generated using "PlotDendrogram" function. The expression patterns of co-expression modules were identified by computing the module eigengenes (MEs) using "ModuleEigengenes" function of hdWGCNA. Module hub genes (highly connected in the co-expression network) were ranked by eigengene-based connectivity (kME) using "PlotKMEs" function. Each module was inspected for maximum coverage and overall expression patterns of co-expressed genes. Using pySCENIC[57] the regulons of each co-expression module was investigated.

Pseudotime analysis of combined fibroblast and myeloid cell subclusters

Obtained subclusters for combined fibroblast and myeloid cells were investigated for their sub-branch association analysis across FS, HGG and MS using Monocle3.[79] Briefly, combined and re-clustered Seurat object was stored as monocle object and processed using Monocle3[79,120] as instructed in their user manual (https://cole-trapnell-lab.github.io/monocle3/docs/starting/). Obtained trajectories were used to integrate the cell differentiation trajectories and their cell distribution across the pseudotime space. Pseudotime graph was examined and continued with the ordered cells at Uniform Manifold Approximation and Projection for Dimension Reduction (UMAP)[121] with minimum distance = 0.7 for further analysis. Based on the distribution of ANXA1, FPR1 and SPP1 expressing cells and the connected trajectories in the pseudotime space, subset cells were chosen and then projected as an input for regression analysis in R. Genes significantly associated with pseudotime (q-value<0.05) and expressed in atleast 100 combined fibroblast and myeloid cells were considered for downstream analysis. Significant genes for selected pseudotime were dissected with the differential expression profiles of FS and HGG groups using Venn diagram. Identified common genes were further investigated for their hybrid expression pattern in selected pseudotime space across the Fb and myeloid cells using 'plot_genes_in_pseudotime' module of Monocle3.

TNT2.0 and murine wound experiments

Excisional splinted wounds (6 mm in diameter) were created on the dorsal skin of C57BL6 as previously described by our group.[24] Briefly, the dorsal side of the mice was naired and cleaned using betadine under anesthesia. Two 6-mm–diameter full-thickness (skin and panniculus carnosus) excisional wounds were made on the dorsal skin with a 6-mm disposable biopsy punch. A donut-shaped splint with an 8-mm inner diameter was made from an 0.5-mm–thick silicone sheet (Grace BioLaboratories, Bend, OR) and placed on the wound using an immediate-bonding adhesive, followed by interrupted 5-0 nylon sutures (Ethicon, Somerville, NJ), such that the wound was centered within the splint. The wound was covered with semiocclusive dressing (Tegaderm; 3M, St. Paul, MN). The animals were euthanized at specific times by CO_2 asphyxiation, and wound tissues were harvested for molecular and histological analysis. *In vivo* TNT2.0 was performed as described previously with a modification in the chip design.[50–53] The hollow microneedle array was fabricated on a double side polished silicon wafer using a standard semiconductor process in a cleanroom environment. The wafer was then transferred to another plasma etching system to perform a deep Si etching called the Bosch process, a common semiconductor process to achieve a vertical etching profile with a high aspect ratio until the hollow microneedles were connected to the reservoirs so that the cargo or the plasmid DNA fluid could freely flow from the reservoir to the hollow microchannel. When an electric pulse was applied between the TNT chip and the tissue, the negatively charged plasma DNA would travel from the reservoir to nearby target cells by electrophoresis and enter them by electroporation.[50–53]

Proximity ligation assay

The proximity of ANXA1 and FPR1 was quantified using PLA (Duolink) that allows the observation of protein-protein interactions. The signal is generated only if the proteins of interest are located within 40nm, therefore detecting interaction.[122] To estimate the PLA signals, the paraffin embedded tissue sections (10 μm) were deparaffinized and processed for PLA analysis as per manufacturer's instructions (Millipore Sigma, USA). Images were collected using a Zeiss Axio Scan fluorescence microscope guided by Zen software (Zeiss).[123] The image data was analyzed for the mean fluorescence intensity of the PLA signals using ImageJ.

QUANTIFICATION AND STATISTICAL ANALYSIS

Quantification and statistical analysis were performed using the Seurat, monocle, CellChat and other packages (See method details) in R. Level of significance of adj. p value per analysis were as indicated with each result or figure legend. Respective figures were generated in R, excel and cytoscape software wherever applicable.